Hydrological variations of the intermediate water masses of the western Mediterranean Sea during the past 20 ka inferred from neodymium isotopic composition in foraminifera and cold-water corals

Quentin Dubois-Dauphin[1], Paolo Montagna[2,3], Giuseppe Siani[1], Eric Douville[4], Claudia Wienberg[5], Dierk Hebbeln[5], Zhifei Liu[6], Nejib Kallel[7], Arnaud Dapoigny[4], Marie Revel[8], Edwige Pons-Branchu[4], Marco Taviani[2,9], Christophe Colin[1]*

[1]Laboratoire Geosciences Paris-Sud (GEOPS), Université de Paris Sud, Université Paris-Saclay, 91405 Orsay, France.
[2]ISMAR-CNR, via Gobetti 101, 40129 Bologna, Italy.
[3]Lamont-Doherty Earth Observatory, Columbia University, 61 Route 9W, Palisades, NY 10964, USA
[4]Laboratoire des Sciences du Climat et de l'Environnement, LSCE/IPSL, CEA-CNRS-UVSQ, Université Paris-Saclay, F-91191 Gif-sur-Yvette, France.
[5]MARUM-Center for Marine Environmental Sciences, University of Bremen, Leobener Strasse, 28359 Bremen, Germany.
[6]State Key Laboratory of Marine Geology, Tongji University, Shanghai 200092, China.
[7]Laboratoire Georessources, Matériaux, Environnements et Changements Globaux, LR13ES23, Faculté des Sciences de Sfax, Université de Sfax, BP1171, 3000 Sfax, Tunisia.
[8]Geoazur, UNS, IRD, OCA, CNRS, 250 rue Albert Einstein, 06500 Valbonne, France
[9]Biology Department, Woods Hole Oceanographic Institution, 266 Woods Hole Road, Woods Hole, MA 02543, USA.

Correspondence to: Christophe Colin (christophe.colin@u-psud.fr)

Abstract. We present the neodymium isotopic composition (εNd) of mixed planktonic foraminifera species from a sediment core collected at 622 m water depth in the Balearic Sea, as well as εNd of scleractinian cold-water corals (CWC; *Madrepora oculata, Lophelia pertusa*) retrieved between 280 and 442 m water depth in the Alboran Sea and at 414 m depth in the South Sardinian continental margin. The aim is to constrain hydrological variations at intermediate depths in the western Mediterranean Sea during the last 20 kyr. Planktonic (*Globigerina bulloides*) and benthic (*Cibicidoides pachyderma*) foraminifera from the Balearic Sea were also analyzed for stable oxygen ($\delta^{18}O$) and carbon ($\delta^{13}C$) isotopes. The foraminiferal and coral εNd values from the Balearic and Alboran Sea are comparable over the last ~13 kyr, with mean values of -8.94±0.26 (1σ; n=24) and -8.91±0.18 (1σ; n=25), respectively. Before 13 ka BP, the foraminiferal εNd values are slightly lower (-9.28±0.15) and tend to reflect higher mixing between intermediate and deep waters, which are characterized by more unradiogenic εNd values. The slight εNd increase after 13 ka BP is associated to a decoupling in the benthic foraminiferal $\delta^{13}C$ composition between intermediate and deeper depths, which started at ~16 ka BP. This suggests an earlier stratification of the water masses and a subsequent reduced contribution of unradiogenic εNd from deep waters. The CWC from the Sardinia Channel show a much larger scatter of εNd values, from -8.66±0.30 to -5.99±0.50, and a lower average (-7.31±0.73; n=19) compared to the CWC and foraminifera from the Alboran and Balearic Sea, indicative of intermediate waters sourced from the Levantine basin. At the time of sapropel S1 deposition (10.2 to 6.4 ka), the εNd values of the Sardinian CWC become more unradiogenic (-8.38±0.47; n=3 at ~8.7 ka BP), suggesting a significant contribution of intermediate waters originated from the

western basin. We propose that western Mediterranean intermediate waters replaced the Levantine Intermediate Water (LIW), and thus a strong reduction of the LIW during the mid-sapropel (~8.7 ka BP). This observation supports a notable change of Mediterranean circulation pattern centered on sapropel S1 that needs further investigations to be confirmed.

1. Introduction

The Mediterranean Sea is a mid-latitude semi-enclosed basin, characterized by evaporation exceeding precipitation and river runoff, where the inflow of fresh and relatively warm surface Atlantic water is transformed into saltier and cooler (i.e. denser) intermediate and deep waters. Several studies have demonstrated that the Mediterranean thermohaline circulation was highly sensitive to both the rapid climatic changes propagated into the basin from high latitudes of the Northern Hemisphere (Cacho et al., 1999, 2000, 2002; Moreno et al., 2002, 2005; Paterne et al., 1999; Martrat et al., 2004; Sierro et al., 2005; Frigola et al., 2007, 2008) and orbitally-forced modifications of the eastern Mediterranean freshwater budget mainly driven by monsoonal river runoff from the subtropics (Rohling et al., 2002; 2004; Bahr et al., 2015). A link between the intensification of the Mediterranean Outflow Water (MOW) and the intensity of the Atlantic Meridional Overturning Circulation (AMOC) was proposed (Cacho et al., 1999, 2000, 2001; Bigg and Wadley, 2001; Sierro et al., 2005; Voelker et al., 2006) and recently supported by new geochemical data in sediments of the Gulf of Cádiz (Bahr et al., 2015). In particular, it has been suggested that the intensity of the MOW and, more generally, the variations of the thermohaline circulation of the Mediterranean Sea could play a significant role in triggering a switch from a weakened to an enhanced state of the AMOC through the injection of saline Mediterranean waters in the intermediate North Atlantic at times of weak AMOC (Rogerson et al., 2006; Voelker et al., 2006; Khélifi et al., 2009). The Mediterranean intermediate waters, notably the Levantine Intermediate Water (LIW), which represent today up to 80 % in volume of the MOW (Kinder and Parilla, 1987) are considered an important driver of MOW-derived salt into the North Atlantic. Furthermore, the LIW also plays a key role in controlling the deep-sea ventilation of the Mediterranean basin, being strongly involved in the formation of deep waters in the Aegean Sea, Adriatic Sea, Tyrrhenian Sea and Gulf of Lions (Millot and Taupier-Letage, 2005). It is hypothesized that a reduction of intermediate and deep-water formation as a consequence of surface hydrological changes in the eastern Mediterranean basin acted as a precondition for the sapropel S1 deposition by limiting the oxygen supply to the bottom waters (De Lange et al., 2008; Rohling et al., 2015; Tachikawa et al., 2015). Therefore, it is crucial to gain a more complete understanding of the variability of the Mediterranean intermediate circulation in the past and its impact on the MOW outflow and, in general, on the Mediterranean thermohaline circulation.

Previous studies have mainly focused on the glacial variability of the deep-water circulation in the western Mediterranean basin (Cacho et al., 2000, 2006; Sierro et al., 2005; Frigola et al., 2007, 2008). During the Last Glacial Maximum (LGM), strong deep-water convection took place in the Gulf of Lions, producing cold, well-ventilated western Mediterranean Deep Water (WMDW) (Cacho et al., 2000, 2006; Sierro et al., 2005), while the MOW flowed at greater depth in the Gulf of Cádiz (Rogerson et al., 2005; Schönfeld and Zahn, 2000). With the onset of the Termination 1 (T1) at about 15 ka, the WMDW production declined until the onset of the Holocene due to the rising sea level, with a relatively weak mode during the Heinrich Stadial 1 (HS1) and the

Younger Dryas (YD) (Sierro et al., 2005; Frigola et al., 2008), that led to the deposition of the Organic Rich Layer 1 (ORL1; 14.5-8.2 ka BP; Cacho et al., 2002).

Because of the disappearance during the Early Holocene of specific epibenthic foraminiferal species, such as *Cibicidoides* spp., which are commonly used for paleohydrological reconstructions, information about the Holocene variability of the deep-water circulation in the western Mediterranean are relatively scarce and are mainly based on grain size analysis and sediment geochemistry (e.g. Frigola et al., 2007). These authors have identified four distinct phases representing different deep-water overturning conditions in the western Mediterranean basin during the Holocene, as well as centennial- to millennial-scale abrupt events of overturning reinforcement.

Faunal and stable isotope records from benthic foraminifera located at intermediate depths in the eastern basin reveal well-ventilated LIW during the last glacial period and deglaciation (Kuhnt et al., 2008; Schmiedl et al., 2010). Similarly, a grain-size record obtained from a sediment core collected within the LIW depth range (~500 m water depth) at the east Corsica margin also documents enhanced bottom currents during the glacial period and for specific time intervals of the deglaciation, such as HS1 and YD (Toucanne et al., 2012). The Early Holocene is characterized by a collapse of the LIW (Kuhnt et al., 2008; Schmiedl et al., 2010; Toucanne et al., 2012) synchronous with the sapropel S1 deposition (10.2 – 6.4 cal ka BP; Mercone et al., 2000). Proxies for deep-water conditions reveal the occurrence of episodes of deep-water overturning reinforcement in the eastern Mediterranean basin at 8.2 ka BP (Rohling et al., 1997, 2015; Kuhnt et al., 2007; Abu-Zied et al., 2008, Siani et al., 2013; Tachikawa et al; 2015), responsible for the interruption of the sapropel S1 in the eastern Mediterranean basin (Mercone et al., 2001; Rohling et al., 2015).

Additional insights into Mediterranean circulation changes may be gained using radiogenic isotopes, such as neodymium, that represent reliable tracers for constraining water-mass mixing and sources (Goldstein and Hemming, 2003, and references therein). It has recently been shown that the neodymium (Nd) isotopic composition, expressed as $\varepsilon Nd = ([(^{143}Nd/^{144}Nd)_{sample} / (^{143}Nd/^{144}Nd)_{CHUR}] - 1) \times 10000$ (CHUR: Chondritic Uniform Reservoir [Jacobsen and Wasserburg , 1980]) of living and fossil scleractinian CWC faithfully traces intermediate and deep-water mass provenance and mixing of the ocean (e.g. van de Flierdt et al., 2010; Colin et al., 2010; López Correa et al., 2012; Monterro-Serrano et al., 2011, 2013; Copard et al., 2012). Differently from the CWC, the εNd composition of fossil planktonic foraminifera is not related to the ambient seawater at calcification depth but reflects the bottom and/or pore water εNd, due to the presence of authigenic Fe-Mn coatings precipitated on their carbonate shell after deposition onto the sediment (Roberts et al., 2010; Elmore et al., 2011; Piotrowski et al., 2012; Tachikawa et al., 2014; Wu et al., 2015). Therefore, the εNd composition of planktonic foraminiferal tests can be used as a useful tracer of deep-water circulation changes in the past, although the effect of pore water on foraminiferal εNd values could potentially complicate the interpretation (Tachikawa et al., 2014).

In the Mediterranean Sea, modern seawater εNd values display a large range from ~-11 to ~-5, and a clear vertical and longitudinal gradient, with more radiogenic values encountered in the eastern basin and typically at intermediate and deeper depths (Spivack and Wasserburg 1988; Henry et al., 1994; Tachikawa et al., 2004; Vance et al., 2004). Considering this large εNd contrast, εNd recorded in fossil CWC and planktonic foraminifera from the Mediterranean offers great potential to trace intermediate and deep-water mass exchange

between the two basins, especially during periods devoid of key epibenthic foraminifera, such as the sapropel S1 or ORL1 events.

Here, the εNd of planktonic foraminifera from a sediment core collected in the Balearic Sea and CWC samples from the Alboran Sea and the Sardinia Channel was investigated to establish past changes of the seawater εNd at intermediate depths and constrain hydrological variations of the LIW during the last ~20 kyr. The εNd values have been combined with stable oxygen ($\delta^{18}O$) and carbon ($\delta^{13}C$) isotope measurements of benthic (*Cibicidoides pachyderma*) and planktonic (*Globigerina bulloides*) foraminifera and sea-surface temperature estimates by modern analogue technique (MAT). Results reveal significant εNd variations at intermediate depths in the western basin interpreted as a drastic reduction of the hydrological exchanges between the western and eastern Mediterranean Sea and the subsequent higher proportion of intermediate water produced in the Gulf of Lions during the time interval corresponding to the sapropel S1 deposition.

2. Seawater εNd distribution in the Mediterranean Sea

The Atlantic Water (AW) enters the Mediterranean Sea as surface inflow through the Strait of Gibraltar with an unradiogenic εNd signature of ~-9.7 in the strait (Tachikawa et al., 2004) and ~-10.4 in the Alboran Sea (Tachikawa et al., 2004, Spivack and Wasserburg, 1988) for depths shallower than 50 m. During its eastward flowing, AW mixes with upwelled Mediterranean Intermediate Water forming the Modified Atlantic Water (MAW) that spreads within the basin (Millot and Taupier-Letage, 2005) (Fig.1). The surface water εNd values (shallower than 50 m) range from -9.8 to -8.8 in the western Mediterranean basin (Henry et al., 1994; Montagna, pers. comm., 2016) and -9.3 to -4.2 in the eastern basin, with seawater off the Nile delta showing the most radiogenic values (Tackikawa et al., 2004; Vance et al., 2004; Montagna, pers. comm., 2016). The surface waters in the eastern Mediterranean basin become denser due to strong mixing and evaporation caused by cold and dry air masses flowing over the Cyprus-Rhodes area in winter, and eventually sink leading to the formation of LIW (Ovchinnikov, 1984; Lascaratos et al., 1993, 1998; Malanotte-Rizzoli et al., 1999; Pinardi and Masetti, 2000). The LIW spreads throughout the entire Mediterranean basin at depths between ~150-200 m and ~600-700 m, and is characterized by more radiogenic εNd values ranging from -7.9 to -4.8 (average value ± 1σ: -6.6 ± 1) in the eastern basin and from -10.4 to -7.58 (-8.7 ± 0.9) in the western basin (Henry et al., 1994; Tachikawa et al., 2004; Vance et al., 2004; Montagna, pers. comm., 2016). The LIW acquires its εNd signature mainly from the partial dissolution of Nile River particles (Tachikawa et al., 2004), which have an average isotopic composition of -3.25 (Weldeab et al., 2002), and the mixing along its path with overlying and underlying water masses with different εNd signatures. The LIW finally enters the Atlantic Ocean at intermediate depths through the Strait of Gibraltar with an average εNd value of -9.2 ± 0.2 (Tachikawa et al., 2004; Montagna, pers. comm., 2016).

The WMDW is formed in the Gulf of Lions due to winter cooling and evaporation followed by mixing between surface waters and the more saline LIW and spreads into the Balearic basin and Tyrrhenian Sea between ~2000 m and 3000 m (Millot, 1999; Schroeder et al., 2013) (Fig. 1). The WMDW is characterized by an average εNd value of -9.4 ± 0.9 (Henry et al., 1994; Tachikawa et al., 2004; Montagna, pers. comm., 2016). Between the WDMW and the LIW (from ~700 to 2000 m), the Tyrrhenian Deep Water (TDW) has been found (Millot et al., 2006), which is produced by the mixing between WMDW and Eastern Mediterranean Deep Water (EMDW) that

cascades in the Tyrrhenian Sea after entering through the Strait of Sicily (Millot, 1999, 2009; Astraldi et al., 2001). The TDW has an average εNd value of -8.1 ± 0.5 (Montagna, pers. comm., 2016).

3. Material and methods

3.1. Cold-water coral and foraminifera samples

Forty-four CWC samples belonging to the species *Lophelia pertusa* and *Madrepora oculata* collected from the Alboran Sea and the Sardinia Channel were selected for this study (Fig. 1). Nineteen fragments were collected at various core depths from a coral-bearing sediment core (RECORD 23; 38°42.18' N; 08°54.75' E; Fig. 1) retrieved from 414 m water depth in the "Sardinian Cold-Water Coral Province" (Taviani et al., 2015) during the R/V Urania cruise "RECORD" in 2013. The core contains well-preserved fragments of *M. oculata* and *L. pertusa* embedded in a brownish muddy to silty carbonate-rich sediment. The Sardinian CWC samples were used for U-series dating and Nd isotopic composition measurements. For the southern Alboran Sea, twenty-five CWC samples were collected at water depths between 280 and 442 m in the "eastern Melilla Coral Province" (Fig. 1) during the R/V Poseidon cruise "POS-385" in 2009 (Hebbeln et al., 2009). Eleven samples were collected at the surface of two coral mounds (New Mound and Horse Mound) and three coral ridges (Brittlestar ridges I, II and III), using a box corer and a remotely operated vehicle (ROV). In addition, fourteen CWC samples were collected from various core depths of three coral-bearing sediment cores (GeoB13728, 13729 and 13730) retrieved from the Brittlestar ridge I. Details on the location of surface samples and cores collected in the southern Alboran Sea and details on the radiocarbon ages obtained from these coral samples are reported in Fink et al. (2013). Like the CWC sample set from the Sardinia Channel, the dated Alboran CWC samples were also used for further Nd isotopic composition analyses in this study.

In addition, a deep-sea sediment core (barren of any CWC fragments) was recovered southwest of the Balearic Sea at 622 m water depth during the R/V Le Suroît cruise "PALEOCINAT II" in 1992 (SU92-33; 35°25.38' N; 0°33.86' E; Fig. 1). The core unit, which consists of 2.1 m of grey to brown carbonaceous clays, was sub-sampled continuously at 5-10 cm intervals for a total number of 24 samples used for $\delta^{18}O$, $\delta^{13}C$ and εNd analyzes.

3.2. Analytical procedures on cold-water coral samples

3.2.1. U/Th dating

The nineteen CWC samples collected from the sediment core RECORD 23 (Sardinia Channel) were analysed for uranium and thorium isotopes to obtain absolute dating using a Thermo Scientific^{TM} Neptune^{Plus} MC-ICPMS installed at the Laboratoire des Sciences du Climat et de l'Environnement (LSCE, Gif-sur-Yvette, France). Prior to analysis, the samples were carefully cleaned using a small diamond blade to remove any visible contamination and sediment-filled cavities. The fragments were examined under a binocular microscope to ensure against the presence of bioeroded zones and finally crushed into a coarse-grained powder with an agate mortar and pestle. The powders (~60-100 mg) were transferred to acid cleaned Teflon beakers, ultrasonicated in MilliQ water, leached with 0.1N HCl for ~ 15 s and finally rinsed twice with MilliQ water. The physically and chemically cleaned samples were dissolved in 3-4 ml dilute HCl (~10%) and mixed with an internal triple spike with known concentrations of ^{229}Th, ^{233}U and ^{236}U, calibrated against a Harwell Uraninite solution (HU-1) assumed to be at secular equilibrium. The solutions were evaporated to dryness at 70°C, redissolved in 0.6 ml 3N HNO_3 and then

loaded into 500 µl columns packed with Eichrom UTEVA resin to isolate uranium and thorium from the other major and trace elements of the carbonate matrix. The U and Th separation and purification followed a procedure slightly modified from Douville et al. (2010). The U and Th isotopes were determined following the protocol recently revisited at LSCE (Pons-Branchu et al., 2014). The ^{230}Th/U ages were calculated from measured atomic ratios through iterative age estimation (Ludwig and Titterington, 1994), using the ^{230}Th, ^{234}U and ^{238}U decay constants of Cheng et al. (2013) and Jaffey et al. (1971). Due to the low ^{232}Th concentration (< 1 ng/g; see Table 1), no correction was applied for the non-radiogenic ^{230}Th fraction.

3.2.2 Nd isotopic composition analyses on cold-water coral fragments

Sub-samples of the CWC fragments from the Sardinia Channel used for U-series dating in this study (Table 1) as well as sub-samples of the twenty-five CWC fragments originating from the Alboran Sea, which were already radiocarbon-dated by Fink et al. (2013) (Table 2), were used for further Nd isotopic composition analyses. The fragments (350 to 600 mg) were subjected to a mechanical and chemical cleaning procedure. The visible contaminations, such as Fe-Mn coatings and detrital particles, were carefully removed from the inner and outermost surfaces of the coral skeletons using a small diamond blade. The physically cleaned fragments were ultrasonicated for 10 min with 0.1 N ultra-clean HCl, followed by several MilliQ water rinses and finally dissolved in 2.5 N ultraclean HNO_3. Nd was separated from the carbonate matrix using Eichrom TRU and LN resins, following the analytical procedure described in detail in Copard et al. (2010).

The ^{143}Nd/^{144}Nd ratios of all purified Nd fractions were analyzed using the ThermoScientific Neptune^{Plus} Multi-Collector Inductively Coupled Plasma Mass Spectrometer (MC-ICP-MS) hosted at LSCE. The mass-fractionation correction was made by normalizing ^{146}Nd/^{144}Nd to 0.7219 and applying an exponential law. During each analytical session, samples were systematically bracketed with analyses of JNdi-1 and La Jolla standard solutions, which are characterised by accepted values of 0.512115±0.000006 (Tanaka et al., 2000) and 0.511855±0.000007 (Lugmair et al., 1983), respectively. Standard JNdi-1 and La Jolla solutions were analysed at concentrations similar to those of the samples (5-10 ppb) and all the measurements affected by instrumental bias were corrected, when necessary, using La Jolla standard. The external reproducibility (2σ) for time resolved measurement, deduced from repeated analyses of La Jolla and JNdi-1 standards, ranged from 0.1 to 0.5 εNd units for the different analytical sessions. The analytical error for each sample analysis was taken as the external reproducibility of the La Jolla standard for each session. Concentrations of Nd blanks were negligible compared to the amount of Nd of CWC investigated in this study.

3.3. Analyses on sediment of core SU92-33

3.3.1. Radiocarbon dating

Radiocarbon dating was measured at UMS-ARTEMIS (Pelletron 3MV) AMS (CNRS-CEA Saclay, France). Seven AMS radiocarbon (^{14}C) dating were performed in first 1.2 m of the core SU92-33 on well-preserved calcareous tests of the planktonic foraminifera *G. bulloides* in the size fraction >150 µm (Table 3). The age model for the core was derived from the calibrated planktonic ages by applying a mean reservoir effect of ~400 years (Siani et al., 2000, 2001). All ^{14}C ages were converted to calendar years (cal. yr BP, BP = AD 1950) by using the INTCAL13 calibration data set (Reimer et al., 2013) and the CALIB 7.0 program (Stuiver and Reimer, 1993).

3.3.2. Stable isotopes

Stable oxygen ($\delta^{18}O$) and carbon ($\delta^{13}C$) isotope measurements were performed in core SU92-33 on well-preserved (clean and intact) samples of the planktonic foraminifera *G. bulloides* (250-315 µm fraction) and the epibenthic foraminifera *C. pachyderma* (250-315 µm fraction) using a Finnigan MAT-253 mass spectrometer at the State Key Laboratory of Marine Geology (Tongji University). Both $\delta^{18}O$ and $\delta^{13}C$ values are presented relative to the Pee Dee Belemnite (PDB) scale by comparison with the National Bureau of Standards (NBS) 18 and 19. The mean external reproducibility was checked by replicate analyses of laboratory standards and is better than ±0.07‰ (1σ) for $\delta^{18}O$ and ±0.04‰ for $\delta^{13}C$.

3.3.3 Nd isotope measurements on planktonic foraminifera

Approximately 25 mg of mixed planktonic foraminifera species were picked from the >63 µm size fraction of each sample already used for stable isotope measurements (Table 4). The samples were gently crushed between glass slides under the microscope to ensure that all chambers were open, and ultrasonicated with MilliQ water. Samples were allowed to settle between ultrasonication steps before removing the supernatant. Each sample was rinsed thoroughly with MilliQ water until the solution was clear and free of clay. The cleaned samples were dissolved in 1N acetic acid and finally centrifuged to ensure that all residual particles were removed, following the procedure described in Roberts et al. (2010). Nd was separated following the analytical procedure reported in Wu et al. (2015). For details on the measurement of Nd isotopes see the section above.

3.3.4. Modern analogue technique (MAT)

The palaeo-sea surface temperatures (SST) were estimated using the modern analogue technique (MAT) (Hutson, 1980; Prell, 1985), implemented by Kallel et al. (1997) for the Mediterranean Sea. This method directly measures the difference between the faunal composition of a fossil sample with a modern database, and it identifies the best modern analogues for each fossil assemblage (Prell, 1985). Reliability of SST reconstructions is estimated using a square chord distance test (dissimilarity coefficient), which represents the mean degree of similarity between the sample and the best 10 modern analogues. When the dissimilarity coefficient is lower than 0.25, the reconstruction is considered to be of good quality (Overpeck et al., 1985; Kallel et al., 1997). For core SU92-33, good dissimilarity coefficients are <0.2, with an average value of ~ 0.13 (varying between 0.07 and 0.19) (Fig. 2a). The calculated mean standard deviation of SST estimates observed in core MD90-917 are ~ 1.5 °C from the late glacial period to the Younger Dryas and ~ 1.2 °C for the Holocene.

4. Results

4.1. Cold-water corals

The good state of preservation for the CWC samples from the Sardinia Channel (RECORD 23; Fig. 1) is attested by their initial $\delta^{234}U$ values (Table 1), which is in the range of the modern seawater value (146.8±0.1; Andersen et al., 2010). If the uncertainty of the $\delta^{234}U_i$ is taken into account, all the values fulfill the so-called "strict" ± 4 ‰ reliability criterion and the U/Th ages can be considered strictly reliable. The coral ages range from 0.091±0.011 to 10.904±0.042 ka BP (Table 1), and reveal three distinct clusters of coral age distribution during the Holocene representing periods of sustained coral occurrence. These periods coincide with the Early Holocene

encompassing a 700-years-lasting time interval from ~10.9 to 10.2 ka BP, the very late Early Holocene at ~8.7 ka BP, and the Late Holocene starting at ~1.5 ka BP (Table 1).

Radiocarbon ages obtained for CWC samples collected in the Alboran Sea were published by Fink et al. (2013) (Table 2). They also document three periods of sustained CWC occurrence coinciding with the Bølling–Allerød (B-A) interstadial (13.5–12.9 cal ka BP), the Early Holocene (11.2–9.8 cal ka BP) and the Mid- to Late Holocene (5.4–0.3 cal ka BP).

The εNd record obtained from the CWC samples from the Alboran Sea displays a narrow range from -9.22±0.30 to -8.59±0.3, which is comparable to the εNd record of the planktonic foraminifera from the Balearic Sea over the last 13.5 kyr (Table 2, Fig. 3b). Most of the CWC εNd values are similar within the analytical error and the record does not reveal any clear difference over the last ~13.5 kyr.

On the contrary, the CWC samples from the Sardinia Channel display a relatively large εNd range, with values varying from -5.99±0.50 to -7.75±0.10 during the Early and Late Holocene, and values as low as -8.66±0.30 during the the mid-sapropel S1 deposition (S1a) at ~8.7 ka BP (Table 1, Fig. 3c).

4.2 Core SU92-33

The stratigraphy of core SU92-33 was derived from the $\delta^{18}O$ variations of the planktonic foraminifera *G. bulloides* (Fig. 2b). The last glacial/interglacial transition and the Holocene encompasses the upper 2.1 m of the core (Fig. 2b). The $\delta^{18}O$ record of *G. bulloides* shows higher values (~3.5 ‰) during the late glacial compared to the Holocene (from ~1.5 to 0.8 ‰) exhibiting a pattern similar to those observed in nearby deep-sea cores from the Western Mediterranean Sea (Sierro et al., 2005; Melki et al., 2009).

The age model for the upper 1.2 m of the core SU92-33 was based on 7 AMS-^{14}C age measurements and a linear interpolation between these ages (Table 3, Fig. 2). For the lower portion of the core, a control point was established at the onset of the last deglaciation, which is coeval in the western and central Mediterranean Sea at ~17 cal ka BP (Sierro et al., 2005; Melki et al., 2009; Siani et al., 2001). Overall, the upper 2.1 m of core SU92-33 spans the last 19 kyr, with an estimated average sedimentation rate ranging from ~15 cm ka^{-1} during the deglaciation to ~10 cm ka^{-1} during the Holocene.

April-May SST reconstruction was derived from MAT to define the main climatic events recorded in core SU92-33 during the last 19 kyr. SST vary from 8.5°C to 17.5°C with high amplitude variability over the last 19 kyr BP (Fig. 2a). The LGM (19-18 ka BP) is characterized by SST values centered at around 12°C. Then, a progressive decrease of ~4°C between 17.8 ka and 16 ka marks the Henrich Stadial 1 (HS1) (Fig. 2a). A warming phase (~14°C) between 14.5 ka BP and 13.8 ka BP coincides with the B-A interstadial and is followed by a cooling (~11°C) between 13.1 ka BP and 11.8 ka BP largely corresponding to the YD (Fig. 2a). During the Holocene, SST show mainly values of ~16°C, with one exception between 7 ka BP and 6 ka BP pointing to an abrupt cooling of ~3°C (Fig. 2a). From the late glacial to the Holocene, SST variations show a similar pattern to that previously observed in the Gulf of Lions and Tyrrhenian Sea (Kallel et al., 1997; Melki et al., 2009) as well as in the Alboran Sea (Martrat et al., 2014; Rodrigo-Gámiz et al., 2014). They are globally synchronous for the main climatic transitions to the well dated South Adriatic Sea core MD90-917 (Siani et al., 2004) confirming the robustness of the SU92-33 age model (Fig. 2a).

The $\delta^{18}O$ and $\delta^{13}C$ records obtained from the benthic foraminifera *C. pachyderma* display significant variations at millennial time scales (Figs. 2c and 2d). The $\delta^{18}O$ values decrease steadily from ~4.5 ‰ during the LGM to ~1.5 ‰ during the Holocene, without showing any significant excursion during HS1 and the YD events (Fig. 2c), in agreement with results obtained from the neighbor core MD99-2343 (Sierro et al., 2005).

The $\delta^{13}C$ record of *C. pachyderma* shows a decreasing trend since the LGM with a low variability from ~1.6 ‰ to ~0.6 ‰ (Fig. 2d). The heaviest $\delta^{13}C$ values are related to the LGM (~1.6 ‰) while the lightest values (~0.6 ‰) characterize the Early Holocene and in particular the period corresponding to the sapropel S1 event in the eastern Mediterranean basin (Fig. 2d).

The εNd values of planktonic foraminifera of core SU92-33 from the Balearic Sea vary within a relatively narrow range between -9.50±0.30 and -8.61±0.30, with an average value of -9.06±0.28 (Table 2, Fig. 3b). The record shows a slight increasing trend since the LGM, with the more unradiogenic values (average -9.28±0.15; n=7) being observed in the oldest part of the record (between 18 and 13.5 ka BP), whereas Holocene values are generally more radiogenic (average -8.84±0.22; n=17) (Fig. 3b).

5. Discussion

Overall, the CWC and foraminiferal εNd values measured in this study point to a pronounced dispersion at intermediate depth in terms of absolute values and variability in Nd isotopes during the Holocene between the Alboran and Balearic Seas and the Sardinia Channel. Furthermore, the foraminiferal εNd record reveals an evolution towards more radiogenic values at intermediate water depth in the Balearic Sea over the last ~19 kyr (Fig. 3).

A prerequisite to properly interpret such εNd differences and variations through time consists in characterizing first the present-day εNd of the main water-mass end-members present in the western Mediterranean basin. It is also necessary to evaluate the temporal changes in εNd of the end-members since the LGM and assess the potential influences of lithogenic Nd input and regional exchange between the continental margins and seawater ("boundary exchange"; Lacan and Jeandel, 2001, 2005) on the εNd values of intermediate water masses.

During its westward flow, the LIW continuously mixes with surrounding waters with different εNd signatures lying above and below. For the western Mediterranean basin, these water masses are the MAW/Western Intermediate Water (WIW) and the TDW/WMDW.As a result, a gradual εNd gradient exists at intermediate depth between the eastern and western Mediterranean basins, with LIW values becoming progressively more unradiogenic towards the Strait of Gibraltar, from -4.8±0.2 at 227 m in the Levantine basin to -10.4±0.2 at 200 m in the Alboran Sea (Tachikawa et al., 2004). Such an εNd pattern implies an effective vertical mixing with more unradiogenetic water masses along the E-W LIW trajectory ruling out severe isotopic modifications of the LIW due to the local exchange between the continental margins and seawater. Unfortunately, no information exists on the potential temporal variability in εNd of the Mediterranean water-mass end-members since the LGM.

It has been demonstrated that eolian dust input can modify the surface and sub-surface εNd distribution of the ocean in some areas (Arsouze et al., 2009). The last glacial period was associated with an aridification of North Africa (Sarnthein et al., 1981; Hooghiemstra et al., 1987; Moreno et al., 2002; Wienberg et al., 2010) and higher fluxes of Saharan dust to the NE tropical Atlantic (Itambi et al., 2009) and the western Mediterranean Sea characterized by unradiogenic εNd values (between -11±0.4 and -14±0.4;; see synthesis in Scheuvens et al., 2013). Bout-Roumazeilles et al. (2013) documented a dominant role of eolian supply in the Siculo-Tunisian

Strait during the last 20 ka, with the exception of a significant riverine contribution (from the Nile River) and a strong reduction of eolian input during the sapropel S1 event. Such variations in the eolian input to the Mediterranean Sea are not associated to a significant change in the seawater εNd record obtained for the Balearic Sea (core SU92-33) during the sapropel S1 event (Fig. 3). Furthermore, the εNd signature of the CWC from the Sardinia Channel (core RECORD 23) shifts to more unradiogenic values (-8.66±0.30) during the sapropel S1 event, which is opposite to what would be expected from a strong reduction of eolian sediment input. In a recent study, Rodrigo-Gámiz et al. (2015) have documented variations in the terrigenous provenance from a sediment record in the Alboran Sea (core 293G; 36°10.414'N, 2°45.280'W, 1840 m water depth) since the LGM. Radiogenic isotopes (Sr, Nd, Pb) point to changes from North African dominated sources during the glacial period to European dominated source during the Holocene. Nevertheless, the major Sr-Nd-Pb excursions documented by Rodrigo-Gámiz et al. (2015) and dated at ca. 11.5, 10.2, 8.9-8.7, 5.6, 2.2 and 1.1. ka cal BP do not seem to affect the εNd values of our foraminifera and coral records.

Taken together, these results suggest that changes of eolian dust input since the LGM cannot explain the observed εNd variability at intermediate water depths.

Consequently, assuming that the Nd isotopic budget of the western Mediterranean Sea has not been strongly modified since the LGM, the reconstructed variations of the E-W gradient of εNd values in the western Mediterranean Sea for the past and notably during the sapropel S1 event (Fig. 3) are indicative of a major reorganization of intermediate water circulation.

5.1 Hydrological changes in the Alboran and Balearic Seas since the LGM

The range in εNd for the CWC from the Alboran Sea (from -9.22±0.30 to -8.8.59±0.30; Table 2) is very close to the one obtained for the planktonic foraminifera from the Balearic Sea (from -9.50±0.30 to -8.61±0.30; Table 4, Fig. 3c), suggesting that both sites are influenced by the same intermediate water masses at least for the last 13.5 kyr BP. Today, LIW occupies a depth range between ~200 and ~700 m in the western Mediterranean basin (Millot, 1999; Sparnocchia et al., 1999). More specifically, the salinity maximum corresponding to the core of LIW is found at around 400 m in the Alboran Sea (Millot, 2009) and up to 550 m in the Balearic Sea (López-Jurado et al., 2008). The youngest CWC sample collected in the Alboran Sea with a rather "recent" age of 0.34 cal ka BP (Fink et al. 2013) displays an εNd value of -8.59±0.30 (Table 2) that is similar to the present-day value of the LIW at the same site (-8.3±0.2) (Dubois-Dauphin et al., submitted) and is significantly different from the WMDW εNd signature in the Alboran Sea (-10.7±0.2, 1270 m water depth; Tachikawa et al., 2004). Considering the intermediate depth range of the studied CWC and foraminifera samples, we can reasonably assume that samples from both sites, in the Balearic Sea (622 m water depth) and in the Alboran Sea (280 to 442 m water depth), record εNd variations of the LIW. The εNd record obtained from planktonic foraminifera generally displays more unradiogenic and homogenous values before ~13 cal ka BP (range from -9.46 to -9.12) compared to the most recent part of the record (range from -9.50 to -8.61), with the highest value of -8.61±0.3 in the Early and Late Holocene.

The SST record displays values centered at around 12°C during the LGM with a subsequent rapid SST decrease towards 9°C , highlighting the onset of the HS1 (Fig. 2a). These values are well comparable to recent high-resolution SST data obtained in the Alboran Sea (Martrat et al., 2014; Rodrigo-Gámiz et al., 2014).

The $\delta^{18}O$ record obtained on *G. bulloides* indicates an abrupt 1‰ excursion towards lighter values centered at about 16 cal ka BP (Table 4), synchronous with the HS1 (Fig. 2b), which is similar to the $\delta^{18}O$ shift reported by Sierro et al. (2005) for a core collected at 2391 m water depth NE of the Balearic Islands (MD99-2343; Fig. 1). As the Heinrich events over the last glacial period are characterized by colder and fresher surface water in the Alboran Sea (Cacho et al., 1999; Pérez-Folgado et al., 2003; Martrat et al., 2004, 2014; Rodrigo-Gámiz et al., 2014) and dry climate on land over the western Mediterranean Sea (Allen et al., 1999; Combourieu-Nebout et al., 2002; Sanchez Goni et al., 2002; Bartov et al., 2003), lighter $\delta^{18}O$ values of planktonic *G. bulloides* are thought to be the result of the inflow of freshwater derived from the melting of icebergs in the Atlantic Ocean into the Mediterranean Sea (Sierro et al., 2005; Rogerson et al., 2008).

During this time interval, the $\delta^{13}C$ record of *C. pachyderma* from the Balearic Sea (core SU92-33) displays a decreasing $\delta^{13}C$ trend after ~16 cal ka BP (from 1.4 ‰ to 0.9 ‰; Table 4; Fig. 4a). Moreover, the $\delta^{13}C$ record obtained on benthic foraminifera *C. pachyderma* from the deep Balearic Sea (core MD99-2343) reveals similar $\delta^{13}C$ values before ~16 cal ka BP suggesting well-mixed and ventilated water masses during the LGM and the onset of the deglaciation (Sierro et al., 2005).

The slightly lower foraminiferal εNd values before ~13 cal ka BP could reflect a stronger influence of water masses deriving from the Gulf of Lions as WMDW (εNd: -9.4±0.9; Henry et al., 1994; Tachikawa et al., 2004; Montagna, pers. comm., 2016). This is in agreement with εNd results obtained by Jiménez-Espejo et al. (2015) from planktonic foraminifera collected from deep-water sites (1989 m and 2382 m) in the Alboran Sea (Fig. 4c). Jiménez-Espejo et al. (2015) documented lower εNd values (ranging from -10.14±0.27 to -9.58±0.22) during the LGM, suggesting an intense deep-water formation. This is also associated to an enhanced activity of the deeper branch of the MOW in the Gulf of Cádiz (Rogerson et al., 2005; Voelker et al., 2006) linked to the active production of the WMDW in the Gulf of Lions during the LGM (Jiménez-Espejo et al., 2015).

The end of the HS1 (14.7 cal ka BP) is concurrent with the onset of the B-A warm interval characterized by increased SST up to 14°C in the Balearic Sea (SU92-33: Fig. 3a), also identified for various sites in the Mediterranean Sea (Cacho et al., 1999; Martrat et al., 2004, 2014; Essallami et al., 2007; Rodrigo-Gámiz et al., 2014). The B-A interval is associated with the so-called melt-water pulse 1A (e.g. Weaver et al., 2003) occurring at around 14.5 cal ka BP. This led to a rapid sea-level rise of about 20 m in less than 500 years and large freshwater discharges in the Atlantic Ocean due to the melting of continental ice sheets (Deschamps et al., 2012), resulting in an enhanced Atlantic inflow across the Strait of Gibraltar. Synchronously, cosmogenic dating of Alpine glacier retreat throughout the western Mediterranean hinterland suggests maximum retreat rates (Ivy-Ochs et al., 2007; Kelly et al., 2006). Overall, these events are responsible for freshening Mediterranean waters and reduced surface water density, and hence, weakened ventilation of intermediate (Toucanne et al., 2012) and deep-water masses (Cacho et al., 2000; Sierro et al., 2005). Similarly, lower benthic $\delta^{13}C$ values obtained for the Balearic Sea (Fig. 4a) point to less ventilated intermediate water relative to the late glacial. In addition, a decoupling in the benthic $\delta^{13}C$ values is observed between deep (MD99-2343) and intermediate (core SU92-33) waters after ~16 cal ka BP (Sierro et al. 2005), suggesting an enhanced stratification of the water masses (Fig. 4a). At this time, the shallowest εNd record from the deep Alboran Sea (core 300G) shifted towards more radiogenic values, while the deepest one (core 304G) remained close to the LGM values (Jimenez-Espejo et al., 2015) (Fig. 4c). Furthermore, results from the UP10 fraction (particles > 10 μm) of the MD99-2343 sediment core (Fig. 4d) indicate a declining bottom-current velocity at 15 ka BP (Frigola et al., 2008). Rogerson et al.

(2008) have hypothesized that during deglacial periods the sinking depth of dense waters produced in the Gulf of Lions was shallower resulting in new intermediate water (WIW) rather than new deep-water (WMDW) as observed today during mild winters (Millot, 1999; Schott et al., 1996). Therefore, intermediate depths of the Balearic Sea could have been isolated from the deep-water with the onset of the T1 (at ~15 ka BP). The reduced convection in the deep western Mediterranean Sea together with the shoaling of the nutricline (Rogerson et al., 2008) led to the deposition of the ORL 1 (14.5 to 8.2 ka B.P; Cacho et al., 2002) and dysoxic conditions below 2000 m in agreement with the absence of epibenthic foraminifera such as *C. pachyderma* after 11 cal ka BP in MD99-2343 (Sierro et al., 2005) (Fig. 4a).

After 13.5 ka BP, planktonic foraminifera εNd values from the Balearic Sea (core SU92-33) become more radiogenic and are in the range of CWC εNd values from the Alboran Sea (Fig. 4b). These values may reveal a stronger influence of the LIW in the Balearic Sea during the Younger Dryas, as also supported by the sortable silt record from the Tyrrhenian Sea (Toucanne et al., 2012) (Fig. 4e). Deeper depths of the Alboran Sea also record a stronger influence of the LIW with an εNd value of -9.1±0.4 (Jimenez-Espejo et al., 2015). In addition, a concomitant activation of the upper MOW branch, as reconstructed from higher values of Zr/Al ratio in sediments of the Gulf of Cádiz, can be related to the enhanced LIW flow in the western Mediterranean Sea (Fig. 4f) (Bahr et al., 2015).

The time of sapropel S1 deposition (10.2 – 6.4 ka) is characterized by a weakening or a shutdown of intermediate- and deep-water formation in the eastern Mediterranean basin (Rossignol-Strick et al., 1982; Cramp and O'Sullivan, 1999; Emeis et al., 2000; Rohling et al., 2015). At this time, planktonic foraminifera εNd values from intermediate water depths in the Balearic Sea (core SU92-33) remain high (between -9.15±0.3 and -8.61±0.3) (Fig. 4b). On the other hand, the deeper Alboran Sea provides a value of -9.8±0.3 pointing to a stronger contribution of WMDW (Jimenez-Espejo et al., 2015), coeval with the recovery of deep-water activity from core MD99-2343 (Frigola et al., 2008).

5.2 Hydrological changes in the Sardinia Channel during the Holocene

The present-day hydrographic structure of the Sardinia Channel is characterized by four water masses, with the surface, intermediate and deep-water masses being represented by MAW, LIW and TDW/WMDW, respectively (Astraldi et al., 2002a; Millot and Taupier-Lepage, 2005). In addition, the WIW, flowing between the MAW and the LIW, has also been observed along the Channel (Sammari et al., 1999). The core of the LIW is located at 400-450 m water depth in the Tyrrhenian Sea (Hopkins, 1988; Astraldi et al., 2002b), which is the depth range of CWC samples from the Sardinia Channel (RECORD 23; 414 m) (Taviani et al., 2015). The youngest CWC sample dated at ~0.1 ka BP has an εNd value of -7.70±0.10 (Table 1, Fig. 5), which is similar within error to the value obtained from a seawater sample collected at 451 m close to the coral sampling location (-8.0±0.4; Montagna, pers. comm., 2016).

The CWC dating from the Sardinia Channel shows three distinct periods of sustained coral occurrence in this area during the Holocene, with each displaying a large variability in εNd values. CWC from the Early Holocene (10.9-10.2 ka BP) and the Late Holocene (<1.5 ka BP) exhibit similar ranges of εNd values (ranging from -5.99±0.50 to -7.75±0.20; Table 1, Fig 5c). Such variations are within the present-day εNd range being characteristic for intermediate waters in the eastern Mediterranean Sea (-6.6±1.0; Tachikawa et al., 2004; Vance et al., 2004). However, the CWC εNd values are more radiogenic than those observed at mid-depth in the

present-day western basin (ranging from -10.4±0.2 to -7.58 ±0.47; Henry et al., 1994; Tachikawa et al., 2004; Montagna, pers. comm., 2016), suggesting a stronger LIW component in the Sardinia Channel during the Early and Late Holocene. The Sardinian CWC εNd variability also reflects the sensitivity of the LIW to changes in the eastern basin such as rapid variability of the Nile River flood discharge (Revel et al., 2014; 2015; Weldeab et al., 2014) or a modification through time in the proportion between the LIW and the Cretan Intermediate Water (CIW). Today, the intermediate water outflowing from the Strait of Sicily is composed by ~66 to 75 % of LIW and 33 to 25 % of CIW (Manca et al., 2006; Millot, 2014). As the CIW is formed in the Aegean Sea, this intermediate water mass is generally more radiogenic than LIW (Tachikawa et al., 2004; Montagna, pers. comm., 2016). Following this hypothesis, a modification of the mixing proportion between the CIW and the LIW may potentially explain values as radiogenic as about -6 in the Sardinia Channel during the Early and Late Holocene (Fig. 5c). However, a stronger LIW and/or a CIW contribution cannot be responsible for εNd values as low as -8.66±0.30 observed during the sapropel S1 event at 8.7 ka BP (Table 1, Fig. 5c). Considering that such unradiogenic value is not observed at intermediate depth in the modern eastern Mediterranean basin, the most plausible hypothesis suggested here is that the CWC were influenced by a higher contribution of intermediate water from the western basin.

5.3 Hydrological implications for the intermediate water masses of the western Mediterranean Sea

The εNd records of the Balearic Sea, Alboran Sea and Sardinia Channel document a temporal variability of the east-west gradient in the western Mediterranean basin during the Holocene. The magnitude of the gradient ranges from ~1.5 to ~3 ε units during the Early and Late Holocene and it is strongly reduced at 8.7 ka BP (from 0 to ~0.5 ε unit), coinciding with the sapropel S1 event affecting the eastern Mediterranean basin (Fig. 5). Such variations could be the result of a modification of the Nd isotopic composition of intermediate water masses due to changes of the LIW production through time and a higher contribution of the western-sourced intermediate water towards the Sardinia Channel coinciding with the sapropel S1 event.

The LIW acquires its radiogenic εNd signature in the Mediterranean Levantine basin mainly from Nd exchange between seawater and lithogenic particles originating mainly from Nile River (Tachikawa et al., 2004). A higher sediment supply from the Nile River starting at ~15 ka BP was documented by a shift to more radiogenic εNd values of the terrigenous fraction obtained from a sediment core having been influenced by the Nile River discharge (Revel et al., 2015) (Fig. 5e). Others studies pointed to a gradual enhanced Nile River runoff as soon as 14.8 ka BP and a peak of Nile discharge from 9.7 to 8.4 ka recorded by large increase in sedimentation rate from 9.7 to 8.4 ka (>120 cm/ka) (Revel et al., 2015; Weldeab et al., 2014; Castaneda et al., 2016). Similarly, enhanced Nile discharge at ~9.5 cal kyr B.P was inferred based on $\delta^{18}O$ in planktonic foraminifera from a sediment core in the southeast Levantine Basin (PS009PC (32°07.7′N, 34°24.4′E; 552 m water depth) (Hennekam et al., 2014). This increasing contribution of the Nile River to the eastern Mediterranean basin has been related to the African Humid Period (14.8–5.5 ka BP; Shanahan et al., 2015), which in turn was linked to the precessional increase in Northern Hemisphere insolation during low eccentricity (deMenocal et al., 2000; Barker et al., 2004; Garcin et al., 2009). An increasing amount of radiogenic sediments dominated by the Blue/Atbara Nile River contribution (Revel et al., 2014) could have modified the εNd of surface water towards more radiogenic values (Revel, pers. comm., 2016). Indeed, planktonic foraminifera εNd values as high as ~ -3 have been documented in the eastern Levantine Basin (ODP site 967; 34°04.27′N, 32°43.53′E; 2553 m water

depth) during the sapropel S1 event as a result of enhanced Nile flooding (Scrivner et al., 2004). The radiogenic signature was likely transferred to intermediate depth as a consequence of the LIW formation in the Rhodes Gyre, and it might have been propagated westwards towards the Sardinia Channel.

Therefore, considering the more unradiogenic value of the CWC samples from the Sardinia Channel during the sapropel S1a event, it is very unlikely that eastern-sourced water flowed at intermediate depth towards the Sardinia Channel. A possible explanation could be the replacement of the radiogenic LIW that was no longer produced in the eastern basin (Rohling, 1994) by less radiogenic western intermediate water (possibly WIW). Such a scenario could even support previous hypotheses of a potential circulation reversal in the eastern Mediterranean from anti-estuarine to estuarine during sapropel formation (Huang and Stanley, 1972; Calvert, 1983; Sarmiento et al., 1988; Buckley and Johnson, 1988; Thunell and Williams, 1989). An alternative hypothesis would be that reduced surface water densities in the eastern Mediterranean during sapropel S1 resulted in the LIW sinking to shallower depths than at present. In this case, CWC from the Sardinia Channel would have been bathed by underlying Western Intermediate Water during the sapropel S1a event.

6. Conclusions

The foraminiferal εNd record from intermediate depths in the Balearic Sea reveals a relatively narrow range of εNd values varying between -9.50 and -8.61 since the LGM (~20 ka). Between 18 and 13.5 cal ka BP, the more unradiogenic εNd values support a vigorous deep overturning in the Gulf of Lions while $\delta^{18}O$ and $\delta^{13}C$ values indicate a stratification of the water masses after 16 cal ka BP. The stratification together with a decrease of the deep-water intensity led to more radiogenic values after ~13 cal ka BP. The foraminiferal εNd record, supported by εNd values from CWC in the Alboran Sea, shows only minor changes in neodymium isotopes from 13.5 cal ka BP to 0.34 cal ka BP, suggesting that the westernmost part of the western Mediterranean basin is not very sensitive to hydrological variations of the LIW.

On the contrary, CWC located at the depth of the LIW in the Sardinia Channel exhibit large εNd variations (between -7.75±0.10 and -5.99±0.50) during the Holocene, suggesting either the role of the Nile River in changing the εNd of the LIW in the eastern Mediterranean basin or a variable LIW/CIW mixing of the water outflowing from the Strait of Sicily. At the time of the sapropel S1 event at ~8.7 ka BP, CWC display a shift toward lower values (-8.66±0.30), similar to those found at intermediate depths in the westernmost part of the western basin. This suggests that western-sourced intermediate water likely filled mid-depth of the southern Sardinia, replacing LIW that was no longer produced (or heavily reduced) in the eastern basin. These results could potentially support a reversal of the Mediterranean circulation, although this assumption needs further investigation to be confirmed.

Acknowledgements

The research leading to this study has received funding from the MISTRALS/PALEOMEX/COFIMED, the French National Research Agency "Investissement d'Avenir" (n°ANR-10-LABX-0018), the HAMOC project ANR-13-BS06-0003 and ENVIMED/Boron Isotope and Trace Elements project. This work contributes to the RITMARE project. We thank Hiske Fink for selecting and kindly providing the cold-water corals samples from the Alboran Sea. We further thank François Thil and Louise Bordier for their support with Nd isotopic

composition analyses. Paolo Montagna is grateful for financial support from the Short Term Mobility Program (CNR). Thanks are also extended to the captains, crews, chief scientists, and scientific parties of research cruises RECORD (R/V Urania), POS-385 (R/V Poseidon) and PALEOCINAT II (R/V Le Suroît).

References

Abu-Zied, R. H., Rohling, E. J., Jorissen, F. J., Fontanier, C., Casford, J. S. L. and Cooke, S.: Benthic foraminiferal response to changes in bottom-water oxygenation and organic carbon flux in the eastern Mediterranean during LGM to Recent times, Mar. Micropaleontol., 67(1-2), 46–68, doi:10.1016/j.marmicro.2007.08.006, 2008.

Allen, J. R. M., Huntley, B., Brandt, U., Brauer, A., Hubberten, H., Keller, J., Kraml, M., Mackensen, A., Mingram, J., Negendank, J. F. W., Nowaczyk, N. R., Oberhänsli, H., Watts, W. A., Wulf, S. and Zolitschka, B.: Rapid environmental changes in southern Europe during the last glacial period, Nature, 400(6746), 740–743, doi:10.1038/23432, 1999.

Andersen, M. B., Stirling, C. H., Zimmermann, B. and Halliday, A. N.: Precise determination of the open ocean 234U/238U composition, Geochemistry, Geophys. Geosystems, 11(12), Q12003, doi:10.1029/2010GC003318, 2010.

Arsouze, T., Dutay, J.-C., Lacan, F. and Jeandel, C.: Reconstructing the Nd oceanic cycle using a coupled dynamical – biogeochemical model, Biogeosciences, 6(12), 2829–2846, doi:10.5194/bg-6-2829-2009, 2009.

Astraldi, M., Gasparini, G. P., Gervasio, L. and Salusti, E.: Dense Water Dynamics along the Strait of Sicily (Mediterranean Sea), J. Phys. Oceanogr., 31(12), 3457–3475, doi:10.1175/1520-0485(2001)031<3457:DWDATS>2.0.CO;2, 2001.

Astraldi, M., Gasparini, G. P., Vetrano, A. and Vignudelli, S.: Hydrographic characteristics and interannual variability of water masses in the central Mediterranean: A sensitivity test for long-term changes in the Mediterranean Sea, Deep. Res. Part I Oceanogr. Res. Pap., 49(4), 661–680, doi:10.1016/S0967-0637(01)00059-0, 2002a.

Astraldi, M., Conversano, F., Civitarese, G., Gasparini, G. P., Ribera d'Alcalà, M. and Vetrano, a.: Water mass properties and chemical signatures in the central Mediterranean region, J. Mar. Syst., 33-34, 155–177, doi:10.1016/S0924-7963(02)00057-X, 2002b.

Bahr, A., Kaboth, S., Jiménez-Espejo, F. J., Sierro, F. J., Voelker, A. H. L., Lourens, L., Röhl, U., Reichart, G. J., Escutia, C., Hernández-Molina, F. J., Pross, J. and Friedrich, O.: Persistent monsoonal forcing of Mediterranean Outflow Water dynamics during the late Pleistocene, Geology, 43(11), 951–954, doi:10.1130/G37013.1, 2015.

Barker, P. A., Talbot, M. R., Street-Perrott, F. A., Marret, F., Scourse, J. and Odada, E. O.: Late Quaternary climatic variability in intertropical Africa, in Past Climate Variability through Europe and Africa, pp. 117–138, Springer Netherlands, Dordrecht., 2004.

595 Bartov, Y., Goldstein, S. L., Stein, M. and Enzel, Y.: Catastrophic arid episodes in the Eastern Mediterranean
596 linked with the North Atlantic Heinrich events, Geology, 31(5), 439, doi:10.1130/0091-
597 7613(2003)031<0439:CAEITE>2.0.CO;2, 2003.

598 Bigg, G. R. and Wadley, M. R.: Millennial-scale variability in the oceans: an ocean modelling view, J. Quat.
599 Sci., 16(4), 309–319, doi:10.1002/jqs.599, 2001.

600 Bout-Roumazeilles, V., Combourieu-Nebout, N., Desprat, S., Siani, G., Turon, J. L. and Essallami, L.: Tracking
601 atmospheric and riverine terrigenous supplies variability during the last glacial and the Holocene in central
602 Mediterranean, Clim. Past, 9(3), 1065–1087, doi:10.5194/cp-9-1065-2013, 2013.

603 Buckley, H. A. and Johnson, L. R.: Late pleistocene to recent sediment deposition in the central and western
604 Mediterranean, Deep Sea Res. Part A. Oceanogr. Res. Pap., 35(5), 749–766, doi:10.1016/0198-0149(88)90028-
605 3, 1988.

606 Cacho, I., Pelejero, C., Grimalt, J. O., Calafat, A. and Canals, M.: C37 alkenone measurements of sea surface
607 temperature in the Gulf of Lions (NW Mediterranean), Org. Geochem., 30(7), 557–566, doi:10.1016/S0146-
608 6380(99)00038-8, 1999.

609 Cacho, I., Grimalt, J. O., Sierro, F. J., Shackleton, N. and Canals, M.: Evidence for enhanced Mediterranean
610 thermohaline circulation during rapid climatic coolings, Earth Planet. Sci. Lett., 183(3-4), 417–429,
611 doi:10.1016/S0012-821X(00)00296-X, 2000.

612 Cacho, I., Grimalt, J. O., Canals, M., Sbaffi, L., Shackleton, N. J., Schönfeld, J. and Zahn, R.: Variability of the
613 western Mediterranean Sea surface temperature during the last 25,000 years and its connection with the Northern
614 Hemisphere climatic changes, Paleoceanography, 16(1), 40–52, doi:10.1029/2000PA000502, 2001.

615 Cacho, I., Grimalt, J. O. and Canals, M.: Response of the Western Mediterranean Sea to rapid climatic variability
616 during the last 50,000 years: a molecular biomarker approach, J. Mar. Syst., 33-34, 253–272,
617 doi:10.1016/S0924-7963(02)00061-1, 2002.

618 Cacho, I., Shackleton, N., Elderfield, H., Sierro, F. J. and Grimalt, J. O.: Glacial rapid variability in deep-water
619 temperature and δ18O from the Western Mediterranean Sea, Quat. Sci. Rev., 25(23-24), 3294–3311,
620 doi:10.1016/j.quascirev.2006.10.004, 2006.

621 Calvert, S. E.: Geochemistry of Pleistocene sapropels and associated sediments from the Eastern Mediterranean,
622 Oceanol. Acta, 6(3), 255–267, 1983.

623 Castañeda, I. S., Schouten, S., Pätzold, J., Lucassen, F., Kasemann, S., Kuhlmann, H. and Schefuß, E.:
624 Hydroclimate variability in the Nile River Basin during the past 28,000 years, Earth Planet. Sci. Lett., 438, 47–
625 56, doi:10.1016/j.epsl.2015.12.014, 2016.

626 Cheng, H., Lawrence Edwards, R., Shen, C.-C., Polyak, V. J., Asmerom, Y., Woodhead, J. D., Hellstrom, J.,
627 Wang, Y., Kong, X., Spötl, C., Wang, X. and Calvin Alexander, E.: Improvements in 230Th dating, 230Th and
628 234U half-life values, and U–Th isotopic measurements by multi-collector inductively coupled plasma mass

spectrometry, Earth Planet. Sci. Lett., 371-372, 82–91, doi:10.1016/j.epsl.2013.04.006, 2013.

Colin, C., Frank, N., Copard, K. and Douville, E.: Neodymium isotopic composition of deep-sea corals from the NE Atlantic: implications for past hydrological changes during the Holocene, Quat. Sci. Rev., 29(19-20), 2509–2517, doi:10.1016/j.quascirev.2010.05.012, 2010.

Combourieu-Nebout, N., Turon, J. L., Zahn, R., Capotondi, L., Londeix, L. and Pahnke, K.: Enhanced aridity and atmospheric high-pressure stability over the western Mediterranean during the North Atlantic cold events of the past 50 k.y, Geology, 30(10), 863–866, doi:10.1130/0091-7613(2002)030<0863:EAAAHP>2.0.CO;2, 2002.

Copard, K., Colin, C., Douville, E., Freiwald, A., Gudmundsson, G., De Mol, B. and Frank, N.: Nd isotopes in deep-sea corals in the North-eastern Atlantic, Quat. Sci. Rev., 29(19-20), 2499–2508, doi:10.1016/j.quascirev.2010.05.025, 2010.

Copard, K., Colin, C., Henderson, G. M., Scholten, J., Douville, E., Sicre, M.-A. and Frank, N.: Late Holocene intermediate water variability in the northeastern Atlantic as recorded by deep-sea corals, Earth Planet. Sci. Lett., 313-314, 34–44, doi:10.1016/j.epsl.2011.09.047, 2012.

Cramp, A. and O'Sullivan, G.: Neogene sapropels in the Mediterranean: a review, Mar. Geol., 153(1-4), 11–28, doi:10.1016/S0025-3227(98)00092-9, 1999.

De Lange, G. J., Thomson, J., Reitz, A., Slomp, C. P., Principato, M. S., Erba, E. and Corselli, C.: Synchronous basin-wide formation and redox-controlled preservation of a Mediterranean sapropel, Nat. Geosci., 1(9), 606–610, 2008.

DeMenocal, P., Ortiz, J., Guilderson, T. and Sarnthein, M.: Coherent High- and Low-Latitude Climate Variability During the Holocene Warm Period, Science (80-.)., 288(5474), 2198–2202, doi:10.1126/science.288.5474.2198, 2000.

Deschamps, P., Durand, N., Bard, E., Hamelin, B., Camoin, G., Thomas, A. L., Henderson, G. M., Okuno, J. and Yokoyama, Y.: Ice-sheet collapse and sea-level rise at the Bølling warming 14,600 years ago, Nature, 483(7391), 559–564, doi:10.1038/nature10902, 2012.

Douville, E., Sallé, E., Frank, N., Eisele, M., Pons-Branchu, E. and Ayrault, S.: Rapid and accurate U–Th dating of ancient carbonates using inductively coupled plasma-quadrupole mass spectrometry, Chem. Geol., 272(1-4), 1–11, doi:10.1016/j.chemgeo.2010.01.007, 2010.

Dubois-Dauphin, Q., Colin, C., Bonneau, L., Montagna, P., Wu, Q., Van Rooij, D., Reverdin, G., Douville, E., Thil, F., Waldner, A., Frank, N.: Fingerprinting North-east Atlantic water masses using Neodymium isotopes, GCA, submitted.

Elmore, A. C., Piotrowski, A. M., Wright, J. D. and Scrivner, A. E.: Testing the extraction of past seawater Nd isotopic composition from North Atlantic deep sea sediments and foraminifera, Geochemistry, Geophys. Geosystems, 12(9), doi:10.1029/2011GC003741, 2011.

663 Emeis, K.-C., Sakamoto, T., Wehausen, R. and Brumsack, H.-J.: The sapropel record of the eastern
664 Mediterranean Sea — results of Ocean Drilling Program Leg 160, Palaeogeogr. Palaeoclimatol. Palaeoecol.,
665 158(3-4), 371–395, doi:10.1016/S0031-0182(00)00059-6, 2000.

666 Fink, H. G., Wienberg, C., De Pol-Holz, R., Wintersteller, P. and Hebbeln, D.: Cold-water coral growth in the
667 Alboran Sea related to high productivity during the Late Pleistocene and Holocene, Mar. Geol., 339, 71–82,
668 doi:10.1016/j.margeo.2013.04.009, 2013.

669 Frigola, J., Moreno, A., Cacho, I., Canals, M., Sierro, F. J., Flores, J. a., Grimalt, J. O., Hodell, D. a. and Curtis,
670 J. H.: Holocene climate variability in the western Mediterranean region from a deepwater sediment record,
671 Paleoceanography, 22(2), n/a–n/a, doi:10.1029/2006PA001307, 2007.

672 Frigola, J., Moreno, A., Cacho, I., Canals, M., Sierro, F. J., Flores, J. A. and Grimalt, J. O.: Evidence of abrupt
673 changes in Western Mediterranean Deep Water circulation during the last 50kyr: A high-resolution marine
674 record from the Balearic Sea, Quat. Int., 181(1), 88–104, doi:10.1016/j.quaint.2007.06.016, 2008.

675 Garcin, Y., Junginger, A., Melnick, D., Olago, D. O., Strecker, M. R. and Trauth, M. H.: Late Pleistocene–
676 Holocene rise and collapse of Lake Suguta, northern Kenya Rift, Quat. Sci. Rev., 28(9-10), 911–925,
677 doi:10.1016/j.quascirev.2008.12.006, 2009.

678 Hebbeln, D, Wienberg, C, Beuck, L, Freiwald, A, Wintersteller, P and cruise participants (2009) Report and
679 preliminary results of R/V POSEIDON Cruise 385 "Cold-water corals of the Alboran Sea (western
680 Mediterranean Sea)", Faro - Toulon, 29.5. - 16.6.2009. Reports of the Department of Geosciences at the
681 University of Bremen, No. 273. Department of Geosciences, Bremen University. urn:nbn:de:gbv:46-
682 ep000106508.

683 Hennekam, R., Jilbert, T., Schnetger, B. and De Lange, G. J.: Solar forcing of Nile discharge and sapropel S1
684 formation in the early to middle Holocene eastern Mediterranean, Paleoceanography, 29(5), 343–356,
685 doi:10.1002/2013PA002553, 2014.

686 Henry, F., Jeandel, C., Dupré, B. and Minster, J.-F.: Particulate and dissolved Nd in the western Mediterranean
687 Sea: Sources, fate and budget, Mar. Chem., 45(4), 283–305, doi:10.1016/0304-4203(94)90075-2, 1994.

688 Hooghiemstra, H., Bechler, A. and Beug, H.-J.: Isopollen maps for 18,000 years B.P. of the Atlantic offshore of
689 northwest Africa: Evidence for paleowind circulation, Paleoceanography, 2, 561–582,
690 doi:10.1029/PA002i006p00561, 1987.

691 Hopkins, T. S.: Recent observations on the intermediate and deep water circulation in the Southern Tyrrhenian
692 Sea, Oceanol. Acta, (Special issue), 41–50, 1988.

693 Huang, T. C. and Stanley, D. J.: Western Alboran sea: sediment dispersal, pounding and reversal of currents, in
694 The Mediterranean Sea: A Natural Sedimentation Laboratory, pp. 521–559, Dowden, Hutchinson & Ross,
695 Stroudsurg, PA., 1972.

696 Hutson, W. H.: The Agulhas Current During the Late Pleistocene: Analysis of Modern Faunal Analogs, Science

(80-.)., 207(4426), 64–66, doi:10.1126/science.207.4426.64, 1980.

Itambi, a. C., von Dobeneck, T., Mulitza, S., Bickert, T. and Heslop, D.: Millennial-scale northwest African droughts related to Heinrich events and Dansgaard-Oeschger cycles: Evidence in marine sediments from offshore Senegal, Paleoceanography, 24(1), PA1205, doi:10.1029/2007PA001570, 2009.

Ivy-Ochs, S., Kerschner, H. and Schlüchter, C.: Cosmogenic nuclides and the dating of Lateglacial and Early Holocene glacier variations: The Alpine perspective, Quat. Int., 164-165, 53–63, doi:10.1016/j.quaint.2006.12.008, 2007.

Jacobsen, S. B. and Wasserburg, G. J.: Sm-Nd isotopic evolution of chondrites, Earth Planet. Sci. Lett., 50(1), 139–155, doi:10.1016/0012-821X(80)90125-9, 1980.

Jaffey, A. H., Flynn, K. F., Glendenin, L. E., Bentley, W. C. and Essling, A. M.: Precision measurements of half-lives and specific activities of 235U and 238U, Phys. Rev. C, 4(5), 1889–1906, doi:10.1103/PhysRevC.4.1889, 1971.

Jiménez-Espejo, F. J., Pardos-Gené, M., Martínez-Ruiz, F., García-Alix, A., van de Flierdt, T., Toyofuku, T., Bahr, A. and Kreissig, K.: Geochemical evidence for intermediate water circulation in the westernmost Mediterranean over the last 20kyrBP and its impact on the Mediterranean Outflow, Glob. Planet. Change, 135, 38–46, doi:10.1016/j.gloplacha.2015.10.001, 2015.

Kallel, N., Paterne, M., Labeyrie, L., Duplessy, J.-C. and Arnold, M.: Temperature and salinity records of the Tyrrhenian Sea during the last 18,000 years, Palaeogeogr. Palaeoclimatol. Palaeoecol., 135(1-4), 97–108, doi:10.1016/S0031-0182(97)00021-7, 1997.

Kelly, M. A., Ivy-Ochs, S., Kubik, P. W., Von Blanckenburg, F. and Schlüchter, C.: Chronology of deglaciation based on 10 Be dates of glacial erosional features in the Grimsel Pass region, central Swiss Alps, Boreas, 35(4), 634–643, doi:10.1111/j.1502-3885.2006.tb01169.x, 2006.

Khelifi, N., Sarnthein, M., Andersen, N., Blanz, T., Frank, M., Garbe-Schonberg, D., Haley, B. a., Stumpf, R. and Weinelt, M.: A major and long-term Pliocene intensification of the Mediterranean outflow, 3.5-3.3 Ma ago, Geology, 37(9), 811–814, doi:10.1130/G30058A.1, 2009.

Kinder, T. H. and Parrilla, G.: Yes, some of the Mediterranean water does come from great depth, J. Geophys. Res., 92, 2901–2906, doi:10.1029/JC092iC03p02901, 1987.

Kuhnt, T., Schmiedl, G., Ehrmann, W., Hamann, Y. and Hemleben, C.: Deep-sea ecosystem variability of the Aegean Sea during the past 22 kyr as revealed by Benthic Foraminifera, Mar. Micropaleontol., 64(3-4), 141–162, doi:10.1016/j.marmicro.2007.04.003, 2007.

Kuhnt, T., Schmiedl, G., Ehrmann, W., Hamann, Y. and Andersen, N.: Stable isotopic composition of Holocene benthic foraminifers from the Eastern Mediterranean Sea: Past changes in productivity and deep water oxygenation, Palaeogeogr. Palaeoclimatol. Palaeoecol., 268(1-2), 106–115, doi:10.1016/j.palaeo.2008.07.010, 2008.

731 Lacan, F. and Jeandel, C.: Tracing Papua New Guinea imprint on the central Equatorial Pacific Ocean using
732 neodymium isotopic compositions and Rare Earth Element patterns, Earth Planet. Sci. Lett., 186(3-4), 497–512,
733 doi:10.1016/S0012-821X(01)00263-1, 2001.

734 Lacan, F. and Jeandel, C.: Neodymium isotopes as a new tool for quantifying exchange fluxes at the continent–
735 ocean interface, Earth Planet. Sci. Lett., 232(3-4), 245–257, doi:10.1016/j.epsl.2005.01.004, 2005.

736 Lascaratos, A. and Nittis, K.: A high-resolution three-dimensional numerical study of intermediate water
737 formation in the Levantine Sea, J. Geophys. Res., 103(C9), 18497, doi:10.1029/98JC01196, 1998.

738 Lascaratos, A., Williams, R. G. and Tragou, E.: A mixed-layer study of the formation of Levantine intermediate
739 water, J. Geophys. Res., 98(C8), 14739, doi:10.1029/93JC00912, 1993.

740 López Correa, M., Montagna, P., Joseph, N., Rüggeberg, A., Fietzke, J., Flögel, S., Dorschel, B., Goldstein, S.
741 L., Wheeler, A. and Freiwald, A.: Preboreal onset of cold-water coral growth beyond the Arctic Circle revealed
742 by coupled radiocarbon and U-series dating and neodymium isotopes, Quat. Sci. Rev., 34, 24–43,
743 doi:10.1016/j.quascirev.2011.12.005, 2012.

744 López-Jurado, J. L., Marcos, M. and Monserrat, S.: Hydrographic conditions affecting two fishing grounds of
745 Mallorca island (Western Mediterranean): during the IDEA Project (2003-2004), J. Mar. Syst., 71(3-4), 303–
746 315, doi:10.1016/j.jmarsys.2007.03.007, 2008.

747 Ludwig, K. R. and Titterington, D. M.: Calculation of 230Th/U isochrons, ages, and errors, Geochim.
748 Cosmochim. Acta, 58(22), 5031–5042, doi:http://dx.doi.org/10.1016/0016-7037(94)90229-1, 1994.

749 Lugmair, G. W., Shimamura, T., Lewis, R. S. and Anders, E.: Samarium-146 in the Early Solar System:
750 Evidence from Neodymium in the Allende Meteorite, Science (80-.)., 222(4627), 1015–1018,
751 doi:10.1126/science.222.4627.1015, 1983.

752 Malanotte-Rizzoli, P., Manca, B. B., D'Alcala, M. R., Theocharis, A., Brenner, S., Budillon, G. and Ozsoy, E.:
753 The Eastern Mediterranean in the 80s and in the 90s: the big transition in the intermediate and deep circulations,
754 Dyn. Atmos. Ocean., 29(2-4), 365–395, doi:10.1016/S0377-0265(99)00011-1, 1999.

755 Manca, B., Ibello, V., Pacciaroni, M., Scarazzato, P. and Giorgetti, A.: Ventilation of deep waters in the Adriatic
756 and Ionian Seas following changes in thermohaline circulation of the Eastern Mediterranean, Clim. Res., 31,
757 239–256, doi:10.3354/cr031239, 2006.

758 Martrat, B., Grimalt, J. O., Lopez-Martinez, C., Cacho, I., Sierro, F. J., Flores, J. A., Zahn, R., Canals, M.,
759 Curtis, J. H. and Hodell, D. a: Abrupt temperature changes in the Western Mediterranean over the past 250,000
760 years., Science (80-.)., 306(5702), 1762–1765, doi:10.1126/science.1101706, 2004.

761 Martrat, B., Jimenez-Amat, P., Zahn, R. and Grimalt, J. O.: Similarities and dissimilarities between the last two
762 deglaciations and interglaciations in the North Atlantic region, Quat. Sci. Rev., 99, 122–134,
763 doi:10.1016/j.quascirev.2014.06.016, 2014.

Melki, T., Kallel, N., Jorissen, F. J., Guichard, F., Dennielou, B., Berné, S., Labeyrie, L. and Fontugne, M.: Abrupt climate change, sea surface salinity and paleoproductivity in the western Mediterranean Sea (Gulf of Lion) during the last 28 kyr, Palaeogeogr. Palaeoclimatol. Palaeoecol., 279(1-2), 96–113, doi:10.1016/j.palaeo.2009.05.005, 2009.

Mercone, D., Thomson, J., Croudace, I. W., Siani, G., Paterne, M. and Troelstra, S.: Duration of S1, the most recent sapropel in the eastern Mediterranean Sea, as indicated by accelerator mass spectrometry radiocarbon and geochemical evidence, Paleoceanography, 15(3), 336–347, doi:10.1029/1999PA000397, 2000.

Mercone, D., Thomson, J., Abu-Zied, R. H., Croudace, I. W. and Rohling, E. J.: High-resolution geochemical and micropalaeontological profiling of the most recent eastern Mediterranean sapropel, Mar. Geol., 177(1-2), 25–44, doi:10.1016/S0025-3227(01)00122-0, 2001.

Millot, C.: Circulation in the Western Mediterranean Sea, J. Mar. Syst., 20(1-4), 423–442, doi:10.1016/S0924-7963(98)00078-5, 1999.

Millot, C.: Another description of the Mediterranean Sea outflow, Prog. Oceanogr., 82(2), 101–124, doi:10.1016/j.pocean.2009.04.016, 2009.

Millot, C.: Heterogeneities of in- and out-flows in the Mediterranean Sea, Prog. Oceanogr., 120, 254–278, doi:10.1016/j.pocean.2013.09.007, 2014.

Millot, C. and Taupier-Letage, I.: Circulation in the Mediterranean Sea, in Environmental Chemistry, vol. 5, edited by A. Saliot, pp. 29–66, Springer Berlin Heidelberg, Heidelberg., 2005.

Millot, C., Candela, J., Fuda, J.-L. and Tber, Y.: Large warming and salinification of the Mediterranean outflow due to changes in its composition, Deep Sea Res. Part I Oceanogr. Res. Pap., 53(4), 656–666, doi:10.1016/j.dsr.2005.12.017, 2006.

Montero-Serrano, J.-C., Frank, N., Colin, C., Wienberg, C. and Eisele, M.: The climate influence on the mid-depth Northeast Atlantic gyres viewed by cold-water corals, Geophys. Res. Lett., 38(19), doi:10.1029/2011GL048733, 2011.

Montero-Serrano, J.-C., Frank, N., Tisnérat-Laborde, N., Colin, C., Wu, C., Lin, K., Shen, C., Copard, K., Orejas, C., Gori, A., De Mol, L., Van Rooij, D., Reverdin, G. and Douville, E.: Decadal changes in the mid-depth water mass dynamic of the Northeastern Atlantic margin (Bay of Biscay), Earth Planet. Sci. Lett., 364, 134–144, doi:10.1016/j.epsl.2013.01.012, 2013.

Moreno, A., Cacho, I., Canals, M., Prins, M. a., Sánchez-Goñi, M.-F., Grimal, O. J. and Weltje, G. J.: Saharan Dust Transport and High-Latitude Glacial Climatic Variability: The Alboran Sea Record, Quat. Res., 58, 318–328, doi:10.1006/qres.2002.2383, 2002.

Moreno, A., Cacho, I., Canals, M., Grimalt, J. O., Sánchez-Goñi, M. F., Shackleton, N. and Sierro, F. J.: Links between marine and atmospheric processes oscillating on a millennial time-scale. A multi-proxy study of the last 50,000yr from the Alboran Sea (Western Mediterranean Sea), Quat. Sci. Rev., 24(14-15), 1623–1636,

799 doi:10.1016/j.quascirev.2004.06.018, 2005.

800 Myers, P. G., Haines, K. and Rohling, E. J.: Modeling the paleocirculation of the Mediterranean: The Last
801 Glacial Maximum and the Holocene with emphasis on the formation of sapropel S1, Paleoceanography, 13(6),
802 586–606, doi:10.1029/98PA02736, 1998.

803 Ovchinnikov, I. M.: The formation of intermediate water in the Mediterranean, Oceanology, 24, 168–173, 1984.

804 Overpeck, J. T., Webb, T. and Prentice, I. C.: Quantitative interpretation of fossil pollen spectra: Dissimilarity
805 coefficients and the method of modern analogs, Quat. Res., 23(1), 87–108, doi:10.1016/0033-5894(85)90074-2,
806 1985.

807 Paterne, M., Kallel, N., Labeyrie, L., Vautravers, M., Duplessy, J.-C., Rossignol-Strick, M., Cortijo, E., Arnold,
808 M. and Fontugne, M.: Hydrological relationship between the North Atlantic Ocean and the Mediterranean Sea
809 during the past 15-75 kyr, Paleoceanography, 14(5), 626–638, doi:10.1029/1998PA900022, 1999.

810 Pérez-Folgado, M., Sierro, F. J., Flores, J. A., Cacho, I., Grimalt, J. O., Zahn, R. and Shackleton, N.: Western
811 Mediterranean planktonic foraminifera events and millennial climatic variability during the last 70 kyr, Mar.
812 Micropaleontol., 48(1-2), 49–70, doi:10.1016/S0377-8398(02)00160-3, 2003.

813 Pinardi, N. and Masetti, E.: Variability of the large scale general circulation of the Mediterranean Sea from
814 observations and modelling: a review, Palaeogeogr. Palaeoclimatol. Palaeoecol., 158(3-4), 153–173,
815 doi:10.1016/S0031-0182(00)00048-1, 2000.

816 Piotrowski, A. M., Galy, A., Nicholl, J. a. L., Roberts, N. L., Wilson, D. J., Clegg, J. a. and Yu, J.:
817 Reconstructing deglacial North and South Atlantic deep water sourcing using foraminiferal Nd isotopes, Earth
818 Planet. Sci. Lett., 357-358, 289–297, doi:10.1016/j.epsl.2012.09.036, 2012.

819 Pons-Branchu, E., Douville, E., Roy-Barman, M., Dumont, E., Branchu, P., Thil, F., Frank, N., Bordier, L. and
820 Borst, W.: A geochemical perspective on Parisian urban history based on U–Th dating, laminae counting and
821 yttrium and REE concentrations of recent carbonates in underground aqueducts, Quat. Geochronol., 24, 44–53,
822 doi:10.1016/j.quageo.2014.08.001, 2014.

823 Prell, W. L.: Stability of low-latitude sea-surface temperatures: an evaluation of the CLIMAP reconstruction
824 with emphasis on the positive SST anomalies. Final report, Providence, RI (USA)., 1985.

825 Reimer, P. J., Bard, E., Bayliss, A., Beck, J. W., Blackwell, P. G., Bronk Ramsey, C., Grootes, P. M.,
826 Guilderson, T. P., Haflidason, H., Hajdas, I., HattŽ, C., Heaton, T. J., Hoffmann, D. L., Hogg, A. G., Hughen, K.
827 A., Kaiser, K. F., Kromer, B., Manning, S. W., Niu, M., Reimer, R. W., Richards, D. A., Scott, E. M., Southon,
828 J. R., Staff, R. A., Turney, C. S. M., & van der Plicht, J. (2013). IntCal13 and Marine13 Radiocarbon Age
829 Calibration Curves 0-50,000 Years cal BP. *Radiocarbon, 55*(4).

830 Revel, M., Colin, C., Bernasconi, S., Combourieu-Nebout, N., Ducassou, E., Grousset, F. E., Rolland, Y.,
831 Migeon, S., Bosch, D., Brunet, P., Zhao, Y. and Mascle, J.: 21,000 Years of Ethiopian African monsoon
832 variability recorded in sediments of the western Nile deep-sea fan, Reg. Environ. Chang., 14(5), 1685–1696,

833 doi:10.1007/s10113-014-0588-x, 2014.

834 Revel, M., Ducassou, E., Skonieczny, C., Colin, C., Bastian, L., Bosch, D., Migeon, S. and Mascle, J.: 20,000
835 years of Nile River dynamics and environmental changes in the Nile catchment area as inferred from Nile upper
836 continental slope sediments, Quat. Sci. Rev., 130, 200–221, doi:10.1016/j.quascirev.2015.10.030, 2015.

837 Roberts, N. L., Piotrowski, A. M., McManus, J. F. and Keigwin, L. D.: Synchronous deglacial overturning and
838 water mass source changes., Science, 327(2010), 75–78, doi:10.1126/science.1178068, 2010.

839 Rodrigo-Gámiz, M., Martínez-Ruiz, F., Rampen, S. W., Schouten, S. and Sinninghe Damsté, J. S.: Sea surface
840 temperature variations in the western Mediterranean Sea over the last 20 kyr: A dual-organic proxy (U K′ 37 and
841 LDI) approach, Paleoceanography, 29(2), 87–98, doi:10.1002/2013PA002466, 2014.

842 Rodrigo-Gámiz, M., Martínez-Ruiz, F., Chiaradia, M., Jiménez-Espejo, F. J. and Ariztegui, D.: Radiogenic
843 isotopes for deciphering terrigenous input provenance in the western Mediterranean, Chem. Geol., 410, 237–250,
844 doi:10.1016/j.chemgeo.2015.06.004, 2015.

845 Rogerson, M., Rohling, E. J., Weaver, P. P. E. and Murray, J. W.: Glacial to interglacial changes in the settling
846 depth of the Mediterranean Outflow plume, Paleoceanography, 20(3), doi:10.1029/2004PA001106, 2005.

847 Rogerson, M., Rohling, E. J. and Weaver, P. P. E.: Promotion of meridional overturning by Mediterranean-
848 derived salt during the last deglaciation, Paleoceanography, 21(4), 1–8, doi:10.1029/2006PA001306, 2006.

849 Rogerson, M., Cacho, I., Jimenez-Espejo, F., Reguera, M. I., Sierro, F. J., Martinez-Ruiz, F., Frigola, J. and
850 Canals, M.: A dynamic explanation for the origin of the western Mediterranean organic-rich layers,
851 Geochemistry, Geophys. Geosystems, 9(7), n/a–n/a, doi:10.1029/2007GC001936, 2008.

852 Rohling, E. J.: Review and new aspects concerning the formation of eastern Mediterranean sapropels, Mar.
853 Geol., 122(1-2), 1–28, doi:10.1016/0025-3227(94)90202-X, 1994.

854 Rohling, E. J., Jorissen, F. J. and De stigter, H. C.: 200 Year interruption of Holocene sapropel formation in the
855 Adriatic Sea, J. Micropalaeontology, 16(2), 97–108, doi:10.1144/jm.16.2.97, 1997.

856 Rohling, E. J., Mayewski, P. a, Abu-Zied, R. H., Casford, J. S. L. and Hayes, A.: Holocene atmosphere-ocean
857 interactions: records from Greenland and the Aegean Sea, Clim. Dyn., 18(7), 587–593, doi:10.1007/s00382-001-
858 0194-8, 2002.

859 Rohling, E. J., Sprovieri, M., Cane, T., Casford, J. S. ., Cooke, S., Bouloubassi, I., Emeis, K. C., Schiebel, R.,
860 Rogerson, M., Hayes, A., Jorissen, F. . and Kroon, D.: Reconstructing past planktic foraminiferal habitats using
861 stable isotope data: a case history for Mediterranean sapropel S5, Mar. Micropaleontol., 50(1-2), 89–123,
862 doi:10.1016/S0377-8398(03)00068-9, 2004.

863 Rohling, E. J., Marino, G. and Grant, K. M.: Mediterranean climate and oceanography, and the periodic
864 development of anoxic events (sapropels), Earth-Science Rev., 143, 62–97, doi:10.1016/j.earscirev.2015.01.008,
865 2015.

Rossignol-Strick, M., Nesteroff, W., Olive, P. and Vergnaud-Grazzini, C.: After the deluge: Mediterranean stagnation and sapropel formation, Nature, 295(5845), 105–110, doi:10.1038/295105a0, 1982.

Sammari, C., Millot, C., Taupier-Letage, I., Stefani, A. and Brahim, M.: Hydrological characteristics in the Tunisia–Sardinia–Sicily area during spring 1995, Deep Sea Res. Part I Oceanogr. Res. Pap., 46(10), 1671–1703, doi:10.1016/S0967-0637(99)00026-6, 1999.

Sarmiento, J. L., Herbert, T. and Toggweiler, J. R.: Mediterranean nutrient balance and episodes of anoxia, Global Biogeochem. Cycles, 2(4), 427–444, doi:10.1029/GB002i004p00427, 1988.

Sánchez-Goñi, M., Cacho, I., Turon, J. L., Guiot, J., Sierro, F. J., Peypouquet, J., Grimalt, J. O. and Shackleton, N. J.: Synchroneity between marine and terrestrial responses to millennial scale climatic variability during the last glacial period in the Mediterranean region, Clim. Dyn., 19(1), 95–105, doi:10.1007/s00382-001-0212-x, 2002.

Sarnthein, M., Tetzlaff, G., Koopmann, B., Wolter, K. and Pflaumann, U.: Glacial and interglacial wind regimes over the eastern subtropical Atlantic and North-West Africa, Nature, 293, 193–196, doi:10.1038/293193a0, 1981.

Scheuvens, D., Schütz, L., Kandler, K., Ebert, M. and Weinbruch, S.: Bulk composition of northern African dust and its source sediments — A compilation, Earth-Science Rev., 116, 170–194, doi:10.1016/j.earscirev.2012.08.005, 2013.

Schmiedl, G., Kuhnt, T., Ehrmann, W., Emeis, K. C., Hamann, Y., Kotthoff, U., Dulski, P. and Pross, J.: Climatic forcing of eastern Mediterranean deep-water formation and benthic ecosystems during the past 22 000 years, Quat. Sci. Rev., 29(23-24), 3006–3020, doi:10.1016/j.quascirev.2010.07.002, 2010.

Schönfeld, J. and Zahn, R.: Late Glacial to Holocene history of the Mediterranean outflow. Evidence from benthic foraminiferal assemblages and stable isotopes at the Portuguese margin, Palaeogeogr. Palaeoclimatol. Palaeoecol., 159(1-2), 85–111, doi:10.1016/S0031-0182(00)00035-3, 2000.

Schott, F., Visbeck, M., Send, U., Fischer, J., Stramma, L. and Desaubies, Y.: Observations of Deep Convection in the Gulf of Lions, Northern Mediterranean, during the Winter of 1991/92, J. Phys. Oceanogr., 26(4), 505–524, doi:10.1175/1520-0485(1996)026<0505:OODCIT>2.0.CO;2, 1996.

Schroeder, K., Millot, C., Bengara, L., Ben Ismail, S., Bensi, M., Borghini, M., Budillon, G., Cardin, V., Coppola, L., Curtil, C., Drago, A., El Moumni, B., Font, J., Fuda, J. L., García-Lafuente, J., Gasparini, G. P., Kontoyiannis, H., Lefevre, D., Puig, P., Raimbault, P., Rougier, G., Salat, J., Sammari, C., Sánchez Garrido, J. C., Sanchez-Roman, A., Sparnocchia, S., Tamburini, C., Taupier-Letage, I., Theocharis, A., Vargas-Yáñez, M. and Vetrano, A.: Long-term monitoring programme of the hydrological variability in the Mediterranean Sea: a first overview of the HYDROCHANGES network, Ocean Sci., 9(2), 301–324, doi:10.5194/os-9-301-2013, 2013.

Scrivner, A. E., Vance, D. and Rohling, E. J.: New neodymium isotope data quantify Nile involvement in

Mediterranean anoxic episodes, Geology, 32(7), 565, doi:10.1130/G20419.1, 2004.

Shanahan, T. M., McKay, N. P., Hughen, K. A., Overpeck, J. T., Otto-Bliesner, B., Heil, C. W., King, J., Scholz, C. A. and Peck, J.: The time-transgressive termination of the African Humid Period, Nat. Geosci., 8(2), 140–144, doi:10.1038/ngeo2329, 2015.

Siani, G., Paterne, M., Arnold, M., Bard, E., Metivier, B., Tisnerat, N. and Bassinot, F.: Radiocarbon reservoir ages in the Mediterranean Sea and Black Sea, Radiocarbon, 42(2), 271–280 [online] Available from: <Go to ISI>://000089971000010, 2000.

Siani, G., Paterne, M., Michel, E., Sulpizio, R., Sbrana, A., Arnold, M. and Haddad, G.: Mediterranean Sea surface radiocarbon reservoir age changes since the last glacial maximum., Science (80-.)., 294(5548), 1917–1920, doi:10.1126/science.1063649, 2001.

Siani, G., Sulpizio, R., Paterne, M. and Sbrana, A.: Tephrostratigraphy study for the last 18,000 C years in a deep-sea sediment sequence for the South Adriatic, Quat. Sci. Rev., 23(23-24), 2485–2500, doi:10.1016/j.quascirev.2004.06.004, 2004.

Siani, G., Magny, M., Paterne, M., Debret, M., Fontugne, M. (2013) - Paleohydrology reconstruction and Holocene climate variability in the South Adriatic Sea. *Climate of the Past*, 9, 499-515.

Sierro, F. J., Hodell, D. A., Curtis, J. H., Flores, J. A., Reguera, I., Colmenero-Hidalgo, E., Bárcena, M. A., Grimalt, J. O., Cacho, I., Frigola, J. and Canals, M.: Impact of iceberg melting on Mediterranean thermohaline circulation during Heinrich events, Paleoceanography, 20(2), n/a–n/a, doi:10.1029/2004PA001051, 2005.

Sparnocchia, S., Gasparini, G. P., Astraldi, M., Borghini, M. and Pistek, P.: Dynamics and mixing of the Eastern Mediterranean outflow in the Tyrrhenian basin, J. Mar. Syst., 20(1-4), 301–317, doi:10.1016/S0924-7963(98)00088-8, 1999.

Spivack, A. J. and Wasserburg, G. J.: Neodymium isotopic composition of the Mediterranean outflow and the eastern North Atlantic, Geochim. Cosmochim. Acta, 52(12), 2767–2773, doi:10.1016/0016-7037(88)90144-5, 1988.

Stratford, K., Williams, R. G. and Myers, P. G.: Impact of the circulation on Sapropel Formation in the eastern Mediterranean, Global Biogeochem. Cycles, 14(2), 683–695, doi:10.1029/1999GB001157, 2000.

Struiver, M., Reimer, P. J. and Reimer, R.: CALIB 7.0, Radiocarb. Calibration Progr., 2005.

Tachikawa, K., Roy-Barman, M., Michard, A., Thouron, D., Yeghicheyan, D. and Jeandel, C.: Neodymium isotopes in the Mediterranean Sea: comparison between seawater and sediment signals, Geochim. Cosmochim. Acta, 68(14), 3095–3106, doi:10.1016/j.gca.2004.01.024, 2004.

Tachikawa, K., Piotrowski, A. M. and Bayon, G.: Neodymium associated with foraminiferal carbonate as a recorder of seawater isotopic signatures, Quat. Sci. Rev., 88, 1–13, doi:10.1016/j.quascirev.2013.12.027, 2014.

Tanaka, T., Togashi, S., Kamioka, H., Amakawa, H., Kagami, H., Hamamoto, T., Yuhara, M., Orihashi, Y.,

Yoneda, S., Shimizu, H., Kunimaru, T., Takahashi, K., Yanagi, T., Nakano, T., Fujimaki, H., Shinjo, R., Asahara, Y., Tanimizu, M. and Dragusanu, C.: JNdi-1: a neodymium isotopic reference in consistency with LaJolla neodymium, Chem. Geol., 168(3-4), 279–281, doi:10.1016/S0009-2541(00)00198-4, 2000.

Tachikawa, K., Vidal, L., Cornuault, M., Garcia, M., Pothin, A., Sonzogni, C., Bard, E., Menot, G. and Revel, M.: Eastern Mediterranean Sea circulation inferred from the conditions of S1 sapropel deposition, Clim. Past, 11(6), 855–867, doi:10.5194/cp-11-855-2015, 2015.

Taviani, M., Angeletti, L., Canese, S., Cannas, R., Cardone, F., Cau, A., Cau, A. B., Follesa, M. C., Marchese, F., Montagna, P. and Tessarolo, C.: The "Sardinian cold-water coral province" in the context of the Mediterranean coral ecosystems, Deep Sea Res. Part II Top. Stud. Oceanogr., doi:10.1016/j.dsr2.2015.12.008, 2015.

Thunell, R. C. and Williams, D. F.: Glacial–Holocene salinity changes in the Mediterranean Sea: hydrographic and depositional effects, Nature, 338(6215), 493–496, doi:10.1038/338493a0, 1989.

Toucanne, S., Jouet, G., Ducassou, E., Bassetti, M. A., Dennielou, B., Angue Minto'o, C. M., Lahmi, M., Touyet, N., Charlier, K., Lericolais, G. and Mulder, T.: A 130,000-year record of Levantine Intermediate Water flow variability in the Corsica Trough, western Mediterranean Sea, Quat. Sci. Rev., 33, 55–73, doi:10.1016/j.quascirev.2011.11.020, 2012.

Vance, D., Scrivner, A. E. and Beney, P.: The use of foraminifera as a record of the past neodymium isotope composition of seawater, Paleoceanography, 19(2), PA2009, doi:10.1029/2003PA000957, 2004.

van de Flierdt, T., Robinson, L. F. and Adkins, J. F.: Deep-sea coral aragonite as a recorder for the neodymium isotopic composition of seawater, Geochim. Cosmochim. Acta, 74(21), 6014–6032, doi:10.1016/j.gca.2010.08.001, 2010.

Voelker, A. H. L., Lebreiro, S. M., Schönfeld, J., Cacho, I., Erlenkeuser, H. and Abrantes, F.: Mediterranean outflow strengthening during northern hemisphere coolings: A salt source for the glacial Atlantic?, Earth Planet. Sci. Lett., 245, 39–55, doi:10.1016/j.epsl.2006.03.014, 2006.

Weaver, A. J., Saenko, O. a., Clark, P. U. and Mitrovica, J. X.: Meltwater Pulse 1A from Antarctica as a Trigger of the Bolling-Allerod Warm Interval, Science (80-.)., 299(5613), 1709–1713, doi:10.1126/science.1081002, 2003.

Weldeab, S., Emeis, K.-C., Hemleben, C. and Siebel, W.: Provenance of lithogenic surface sediments and pathways of riverine suspended matter in the Eastern Mediterranean Sea: evidence from 143Nd/144Nd and 87Sr/86Sr ratios, Chem. Geol., 186(1-2), 139–149, doi:10.1016/S0009-2541(01)00415-6, 2002.

Weldeab, S., Menke, V. and Schmiedl, G.: The pace of East African monsson evolution during the Holocene, Geophys. Res. Lett., 41, 1724–1731, doi:10.1002/2014GL059361.Received, 2014.

Wienberg, C., Frank, N., Mertens, K. N., Stuut, J.-B. W., Marchant, M., Fietzke, J., Mienis, F. and Hebbeln, D.: Glacial cold-water coral growth in the Gulf of Cádiz: Implications of increased palaeo-productivity, Earth

Planet. Sci. Lett., 298(3-4), 405–416, doi:10.1016/j.epsl.2010.08.017, 2010.

Wu, Q., Colin, C., Liu, Z., Thil, F., Dubois-Dauphin, Q., Frank, N., Tachikawa, K., Bordier, L. and Douville, E.: Neodymium isotopic composition in foraminifera and authigenic phases of the South China Sea sediments: Implications for the hydrology of the North Pacific Ocean over the past 25 kyr, Geochemistry, Geophys. Geosystems, 16(11), 3883–3904, doi:10.1002/2015GC005871, 2015.

Table captions

Table 1. U-series ages and εNd values obtained for cold-water coral samples collected from sediment core RECORD 23 (Sardinia Channel).

Table 2. εNd values obtained for cold-water corals from the southern Alboran Sea. The AMS ^{14}C ages published by Fink et al. (2013) are also reported as Median probability age (ka BP).

Table 3. AMS ^{14}C ages of samples of the planktonic foraminifer *G. bulloides* from 'off-mound' sediment core SU92-33. The AMS ^{14}C ages were corrected for ^{13}C and a mean reservoir age of 400 yrs, and were converted into calendar years using the INTCAL13 calibration data set (Reimer et al., 2013) and the CALIB 7.0 program (Struiver et al., 2005).

Table 4. Multiproxy data obtained for the upper 2.1 m of sediment core SU92-33 (Balearic Sea). Stable oxygen and carbon isotopes were measured on benthic (*C. pachyderma*) and planktonic (*G. bulloides*) foraminifera; εNd values were obtained on mixed planktonic foraminifera samples. The age results from a combination of 7 AMS-^{14}C age measurements for the upper 1.2 m of the core and by a linear interpolation between these ages as well as the δ^{18}O variations of the planktonic foraminifera *G. bulloides.*

Figure captions

Figure 1. Map of the western Mediterranean Sea showing the locations of samples investigated in this study. Yellow dot indicates the sampling location of the sediment core from the Balearic Sea (SU92-33); yellow stars indicate the locations of the CWC-bearing cores from the Sardinia Channel (RECORD 23) and the southern Alboran Sea (for further details on the CWC from the Alboran Sea refer also to Fink et al., 2013). The cores discussed in this paper (Gulf of Cádiz: IODP site U1387, Balearic Sea: MD09-2343, northern Tyrrhenian Sea: MD01-2472, Adriatic Sea: MD90-917) are indicated by black dots, and seawater stations are marked by open squares. Arrows represent the main oceanographic currents. The black line shows the general trajectory of the Modified Atlantic Water (MAW) flowing at the surface from the Atlantic Ocean toward the western and eastern Mediterranean. The orange line represents the Levantine Intermediate Water (LIW) originating from the eastern basin. The black dashed line shows the trajectory of the Western Mediterranean Deep Water (WMDW) flowing from the Gulf of Lions toward the Strait of Gibraltar.

Figure 2. (a) Sea Surface Temperature (SST) records of cores SU92-33 (red line) and MD90-917 (green line; Siani et al., 2004), (b) δ^{18}O record obtained on planktonic foraminifer *G. bulloides* for core SU92-33, (c) δ^{18}O record obtained on benthic foraminifer *C. pachyderma* for core SU92-33, (d) δ^{13}C record obtained on benthic foraminifer *C. pachyderma* for core SU92-33. LGM: Last Glacial Maximum; HS1: Heinrich Stadial 1; B-A: Bølling-Allerød; YD: Younger Dryas. Black triangles indicate AMS ^{14}C age control points.

Figure 3. (a) Sea Surface Temperature (SST) record of core SU92-33 (red line), (b) εNd records obtained on mixed planktonic foraminifers from core SU92-33 (open circles) and from cold-water coral fragments collected in the Alboran Sea (red squares), (c) εNd values of cold-water corals from core RECORD 23 (Sardinia Channel).

Figure 4. (a) $\delta^{13}C$ records obtained on benthic foraminifer *C. pachyderma* for cores SU92-33 (red line) and MD99-2343 (blue line; Sierro et al., 2005). (b) εNd records obtained on mixed planktonic foraminifers from core SU92-33 (open circles) and from cold-water coral fragments collected in the Alboran Sea (red squares). Modern εNd values for LIW (orange dashed line) and WMDW (blue dashed line) are also reported for comparison. (c) εNd values obtained for planktonic foraminifera with Fe-Mn coatings at sites 300G (36°21.532' N, 1°47.507' W; 1860 m; open dots) and 304G (36°19.873' N, 1°31.631' W; 2382 m; black dots) in Alboran Sea (Jimenez-Espejo et al., 2015). (d) UP10 fraction (>10 μm) from core MD99-2343 (Frigola et al., 2008). (e) Sortable silt mean grain-size of core MD01-2472 (Toucanne et al., 2012). (f) Ln Zr/Al ratio at IODP site U1387 (36°48.3' N 7°43.1' W; 559 m) (Bahr et al., 2015).

Figure 5. (a) $\delta^{18}O$ record obtained on planktonic foraminifer *G. bulloides* for core SU92-33, (b) $\delta^{13}C$ records obtained on benthic foraminifer *C. pachyderma* for core SU92-33, (c) εNd values of cold-water corals from core RECORD 23 (Sardinia Channel), (d) εNd values records obtained on mixed planktonic foraminifera from core SU92-33 (open circles) and from cold-water coral fragments collected in the Alboran Sea (red squares), (e) εNd values obtained on terrigenous fraction of MS27PT located close the Nile River mouth in the eastern Mediterranean basin (Revel et al., 2015)

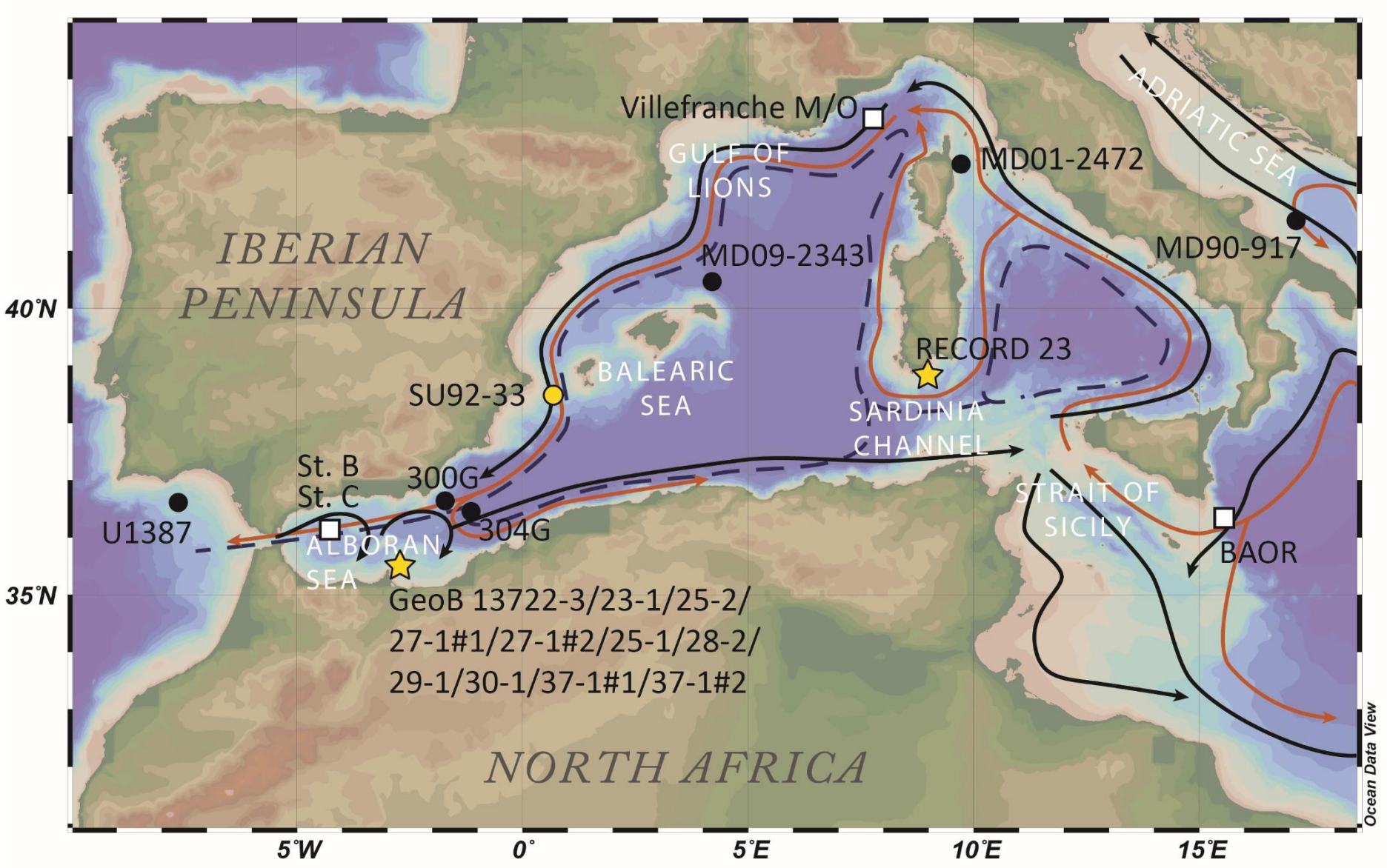
Villefranche M/O
GULF OF LIONS
MD01-2472
ADRIATIC SEA
IBERIAN PENINSULA
MD09-2343
MD90-917
RECORD 23
BALEARIC SEA
SU92-33
SARDINIA CHANNEL
St. B
St. C
300G
304G
U1387
ALBORAN SEA
STRAIT OF SICILY
BAOR
GeoB 13722-3/23-1/25-2/
27-1#1/27-1#2/25-1/28-2/
29-1/30-1/37-1#1/37-1#2
NORTH AFRICA
40˚N
35˚N
5˚W
0˚
5˚E
10˚E
15˚E
Ocean Data View

Figure 1

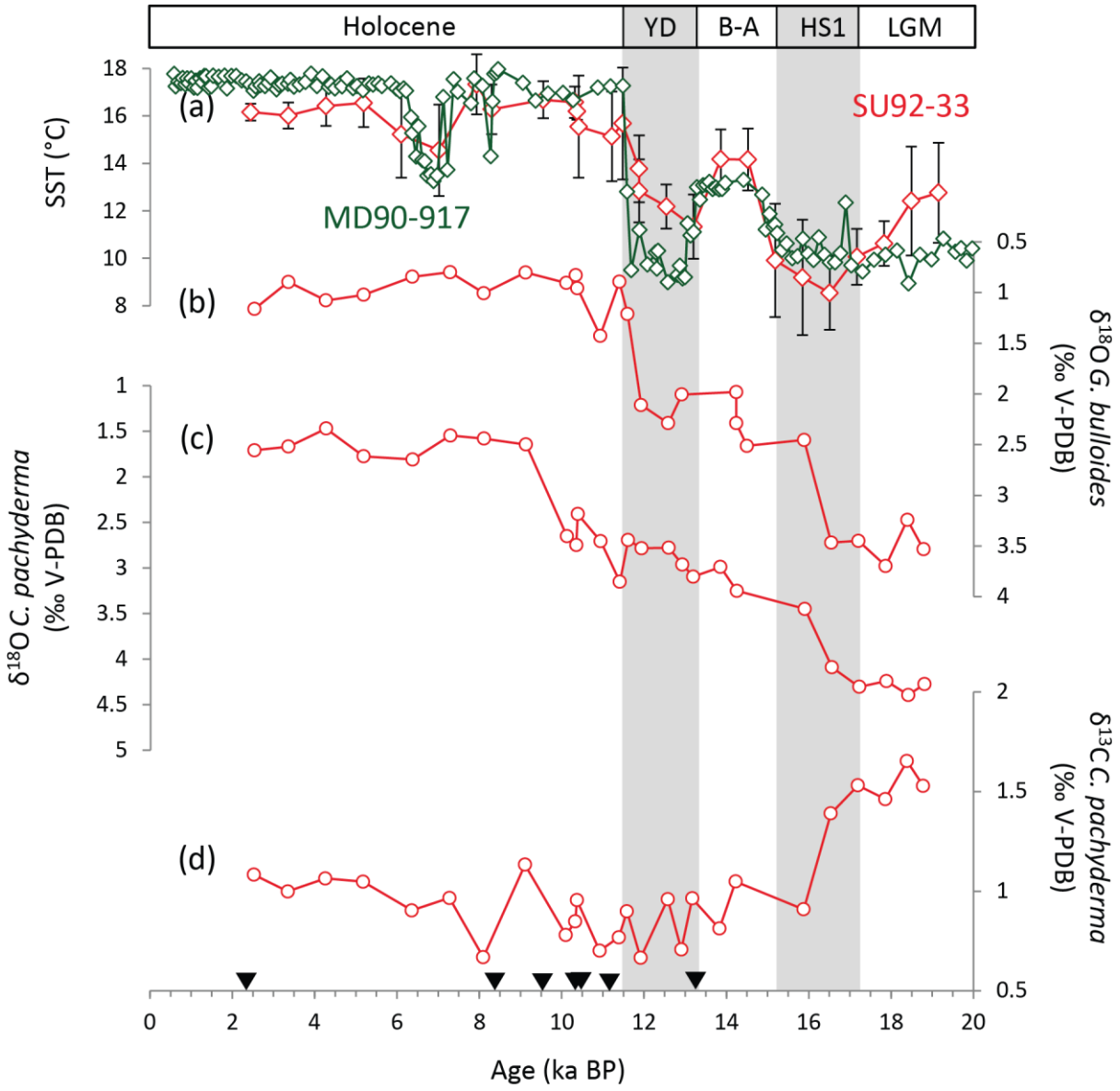
Holocene
YD
B-A
HS1
LGM
(a)
(b)
(c)
(d)
SST (°C)
MD90-917
SU92-33
δ18O G. bulloides (‰ V-PDB)
δ18O C. pachyderma (‰ V-PDB)
δ13C C. pachyderma (‰ V-PDB)
Age (ka BP)

Figure 2

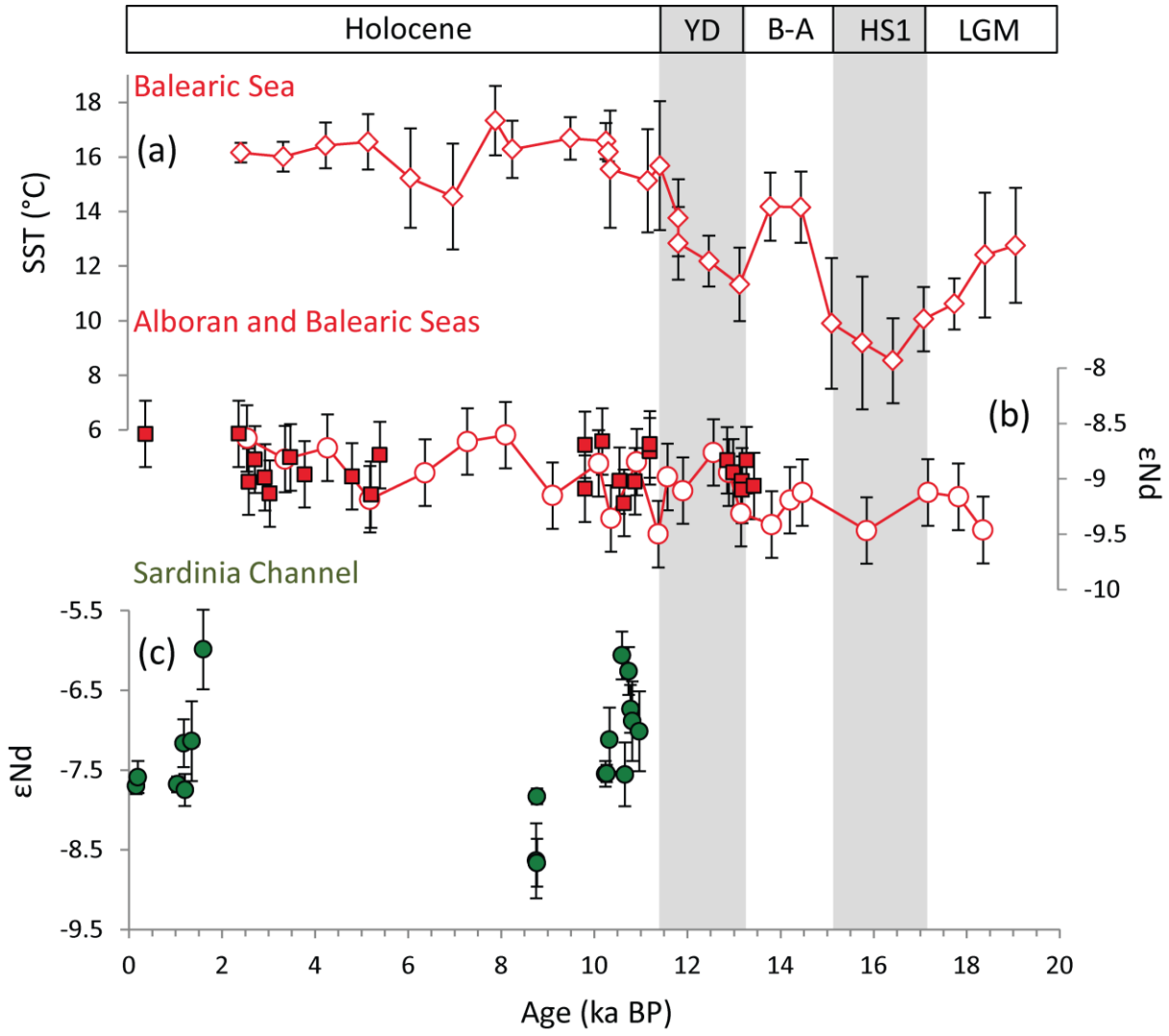
Holocene
YD
B-A
HS1
LGM
Balearic Sea
(a)
SST (°C)
Alboran and Balearic Seas
(b)
εNd
Sardinia Channel
(c)
εNd
Age (ka BP)

Figure 3

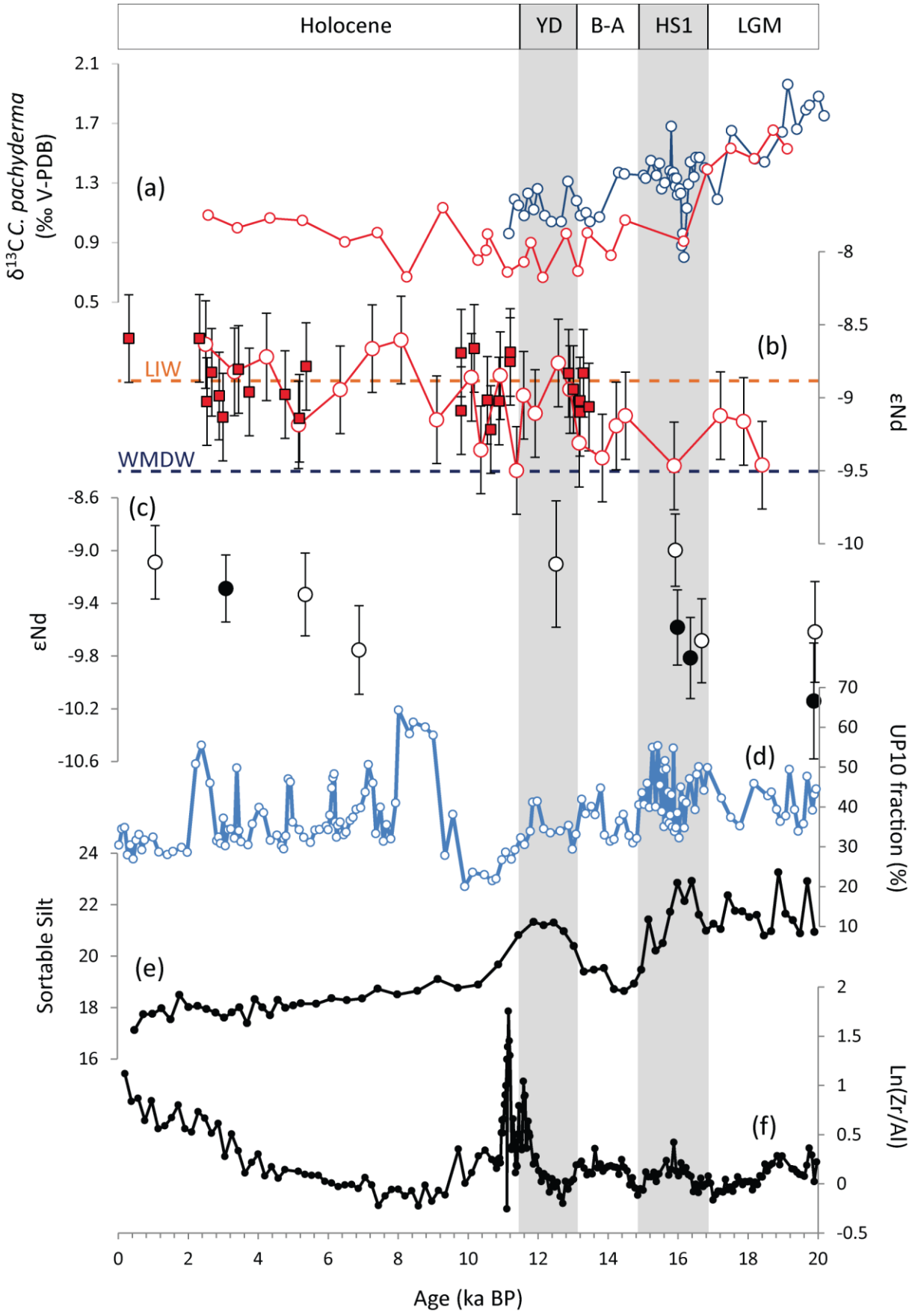
Holocene
YD
B-A
HS1
LGM
(a)
(b)
(c)
(d)
(e)
(f)
LIW
WMDW
δ13C C. pachyderma (‰ V-PDB)
εNd
εNd
UP10 fraction (%)
Sortable Silt
Ln(Zr/Al)
Age (ka BP)

Figure 4

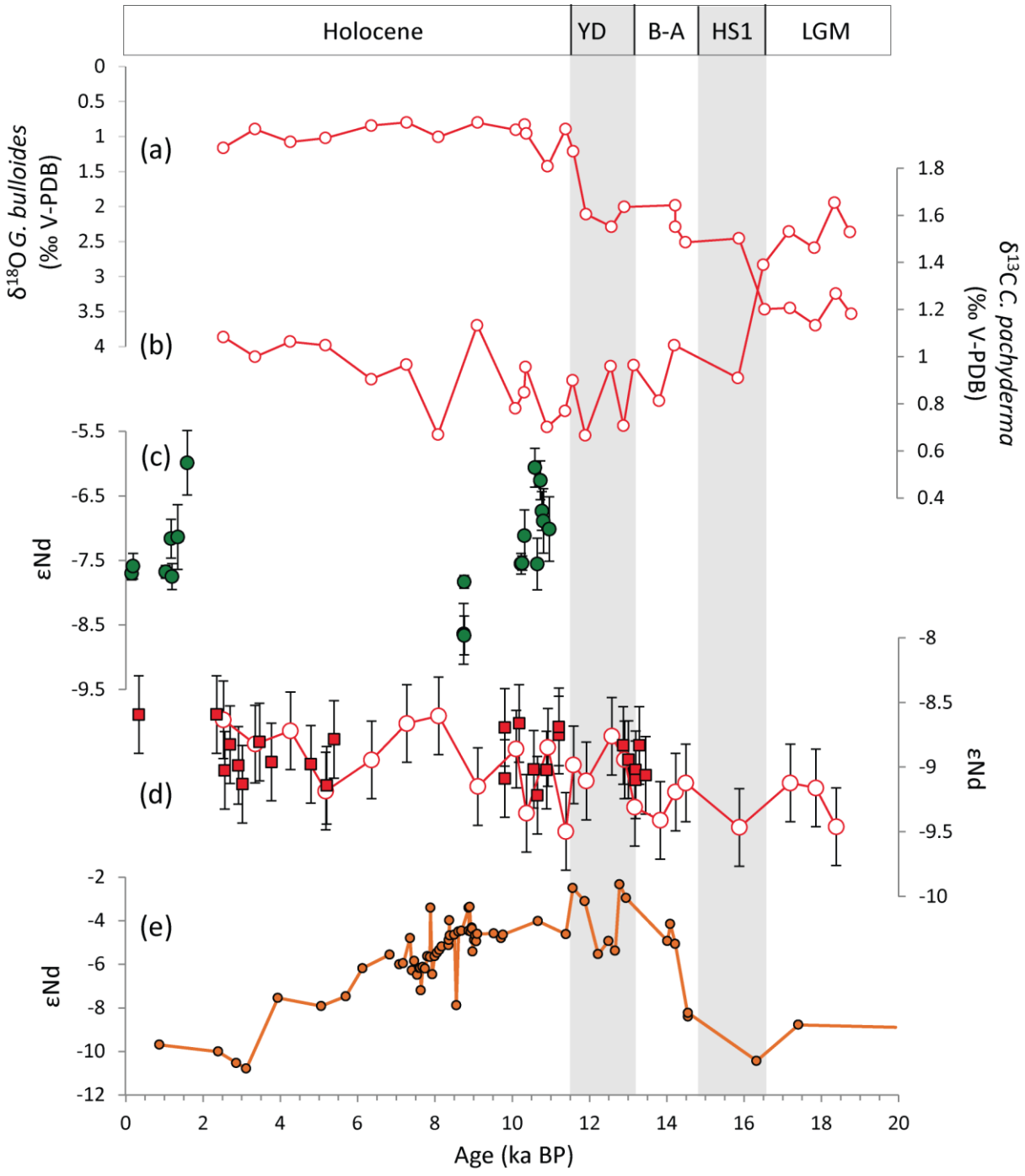
Holocene
YD
B-A
HS1
LGM
(a)
(b)
(c)
(d)
(e)
δ18O G. bulloides (‰ V-PDB)
δ13C C. pachyderma (‰ V-PDB)
εNd
εNd
εNd
Age (ka BP)

Figure 5

Sample ID	Depth in core (cm)	Corals species	^{238}U (µg/g)	^{232}Th (ng/g)	$\delta^{234}U_m$ (‰)	$^{230}Th/^{238}U$	$^{230}Th/^{232}Th$	Age (ka BP)	$\delta^{234}U_{(0)}$ (‰)	$^{143}Nd/^{144}Nd$	εNd
RECORD_23_V	0-3,5	*Madrepora oculata*	3.31 ±0.005	0.68 ±0.014	151.85 ±1.7	0.00163 ±0.00011	25 ±1.7	0.091 ±0.011	151.92 ±1.7	0.512243 ±0.000005	-7.70 ±0.10
RECORD_23_V	3-7	*Madrepora oculata*	3.23 ±0.002	0.52 ±0.001	147.11 ±0.6	0.00199 ±0.00006	38 ±1.1	0.127 ±0.006	147.19 ±0.6	0.512249 ±0.000010	-7.59 ±0.20
RECORD_23_V	7-10	*Madrepora oculata*	3.99 ±0.007	0.25 ±0.002	147.52 ±1.7	0.01227 ±0.00022	640 ±11.6	1.110 ±0.023	148.01 ±1.7	0.512244 ±0.000015	-7.68 ±0.30
RECORD_23_V	8-10	*Madrepora oculata*	3.79 ±0.005	0.41 ±0.001	147.77 ±0.7	0.01253 ±0.00007	350 ±2.0	1.135 ±0.008	148.27 ±0.7	0.512271 ±0.000010	-7.16 ±0.20
RECORD_23_IV	6-9	*Madrepora oculata*	4.06 ±0.006	0.35 ±0.001	148.47 ±1.2	0.01366 ±0.00011	480 ±3.8	1.243 ±0.012	149.02 ±1.2	0.512241 ±0.000010	-7.75 ±0.20
RECORD_23_IV	27-30	*Madrepora oculata*	4.06 ±0.003	1.09 ±0.001	146.91 ±1.3	0.01405 ±0.00013	159 ±1.4	1.283 ±0.014	147.47 ±1.3	0.512272 ±0.000026	-7.14 ±0.50
RECORD_23_IV	37-40	*Madrepora oculata*	3.52 ±0.005	0.08 ±0.000	148.25 ±1.1	0.01663 ±0.00012	2308 ±16.4	1.529 ±0.013	148.92 ±1.1	0.512331 ±0.000026	-5.99 ±0.50
RECORD_23_III	55-57	*Madrepora oculata*	3.63 ±0.002	0.27 ±0.000	145.30 ±0.7	0.08832 ±0.00020	3530 ±8.1	8.685 ±0.027	148.93 ±0.8	0.512195 ±0.000026	-8.64 ±0.50
RECORD_23_III	58-61	*Madrepora oculata*	4.24 ±0.004	0.36 ±0.001	146.71 ±1.2	0.08859 ±0.00037	3336 ±14.0	8.702 ±0.048	150.39 ±1.2	0.512237 ±0.000010	-7.83 ±0.20
RECORD_23_III	63-66	*Lophelia pertusa*	4.15 ±0.005	0.42 ±0.002	147.19 ±0.8	0.08863 ±0.00054	2783 ±17.1	8.703 ±0.063	150.89 ±0.9	0.512194 ±0.000015	-8.66 ±0.30
RECORD_23_I	0-2	*Lophelia pertusa*	3.35 ±0.002	0.37 ±0.000	147.02 ±0.7	0.10283 ±0.00018	2788 ±4.8	10.173 ±0.025	151.34 ±0.7	0.512251 ±0.000010	-7.55 ±0.20
RECORD_23_II	62-65	*Lophelia pertusa*	3.27 ±0.003	0.39 ±0.002	144.75 ±1.2	0.10289 ±0.00061	2721 ±16.1	10.201 ±0.075	149.01 ±1.2	0.512251 ±0.000010	-7.54 ±0.20
RECORD_23_II	50-52	*Lophelia pertusa*	2.92 ±0.003	0.92 ±0.003	145.39 ±1.6	0.10351 ±0.00061	1046 ±6.2	10.260 ±0.079	149.69 ±1.6	0.512273 ±0.000021	-7.12 ±0.40
RECORD_23_I	12-14	*Lophelia pertusa*	3.07 ±0.002	0.49 ±0.000	145.22 ±0.7	0.10609 ±0.00023	1971 ±4.3	10.531 ±0.031	149.64 ±0.7	0.512327 ±0.000015	-6.06 ±0.30
RECORD_23_I	5-7	*Lophelia pertusa*	3.50 ±0.002	0.42 ±0.000	146.35 ±0.9	0.10677 ±0.00016	2654 ±4.0	10.591 ±0.025	150.82 ±0.9	0.512251 ±0.000021	-7.55 ±0.40
RECORD_23_II	94-98	*Lophelia pertusa*	3.14 ±0.003	0.62 ±0.002	146.42 ±1.0	0.10755 ±0.00047	1737 ±7.6	10.672 ±0.059	150.94 ±1.0	0.512317 ±0.000015	-6.26 ±0.30
RECORD_23_I	15-17	*Lophelia pertusa*	3.40 ±0.003	0.46 ±0.000	146.01 ±0.9	0.10790 ±0.00021	2409 ±4.6	10.713 ±0.031	150.53 ±0.9	0.512293 ±0.000015	-6.73 ±0.30
RECORD_23_II	96-100	*Lophelia pertusa*	3.61 ±0.004	0.35 ±0.001	145.50 ±0.8	0.10821 ±0.00044	3579 ±14.7	10.750 ±0.055	150.02 ±0.8	0.512285 ±0.000026	-6.89 ±0.50
RECORD_23_II	93-95	*Lophelia pertusa*	3.19 ±0.003	0.24 ±0.000	143.33 ±0.8	0.10947 ±0.00032	4381 ±12.7	10.904 ±0.042	147.85 ±0.9	0.512279 ±0.000026	-7.01 ±0.50

Table 1

Sample ID	Core depth (cm)	Species	Water Depth (m)	Median probability age (ka BP)	$^{143}Nd/^{144}Nd$	εNd
GeoB 13727-1#1	Surface	*Lophelia pertusa*	363	0.339	0.512198 ±0.000015	-8.59 ±0.30
GeoB 13727-1#2	Surface	*Madrepora oculata*	353	2.351	0.512198 ±0.000015	-8.59 ±0.30
GeoB 13730-1	6	*Lophelia pertusa*	338	2.563	0.512175 ±0.000015	-9.03 ±0.30
GeoB 13728-1	Bulk (0-15)	*Lophelia pertusa*	343	2.698	0.512185 ±0.000015	-8.83 ±0.30
GeoB 13728-2	2	*Lophelia pertusa*	343	2.913	0.512177 ±0.000015	-8.99 ±0.30
GeoB 13722-3	Bulk (0-15)	*Madrepora oculata*	280	3.018	0.512170 ±0.000015	-9.13 ±0.30
GeoB 13722-3	Bulk (15-30)	*Madrepora oculata*	280	3.463	0.512186 ±0.000015	-8.81 ±0.30
GeoB 13735-1	Bulk (0-15)	*Madrepora oculata*	280	3.770	0.512179 ±0.000015	-8.96 ±0.30
GeoB 13723-1	Bulk (0-8)	*Madrepora oculata*	291	4.790	0.512178 ±0.000015	-8.98 ±0.30
GeoB 13725-2	Surface	*Madrepora oculata*	355	5.201	0.512169 ±0.000015	-9.14 ±0.30
GeoB 13723-1	Bulk (8-20)	*Madrepora oculata*	291	5.390	0.512187 ±0.000015	-8.79 ±0.30
GeoB 13729-1	2.5	*Lophelia pertusa*	442	9.810	0.512172 ±0.000015	-9.09 ±0.30
GeoB 13729-1	2.5	*Lophelia pertusa*	442	9.810	0.512193 ±0.000015	-8.69 ±0.30
GeoB 13729-1	49	*Lophelia pertusa*	442	10.181	0.512194 ±0.000015	-8.66 ±0.30
GeoB 13730-1	102	*Lophelia pertusa*	338	10.556	0.512176 ±0.000015	-9.02 ±0.30
GeoB 13730-1	194	*Lophelia pertusa*	338	10.652	0.512165 ±0.000015	-9.22 ±0.30
GeoB 13729-1	315	*Lophelia pertusa*	442	10.889	0.512176 ±0.000015	-9.02 ±0.30
GeoB 13729-1	375	*Lophelia pertusa*	442	11.206	0.512189 ±0.000015	-8.75 ±0.30
GeoB 13730-1	298	*Lophelia pertusa*	338	11.208	0.512193 ±0.000015	-8.69 ±0.30
GeoB 13728-2	191	*Lophelia pertusa*	343	12.874	0.512185 ±0.000015	-8.83 ±0.30
GeoB 13737-1#2	Surface	*Lophelia pertusa*	297	13.005	0.512180 ±0.000015	-8.94 ±0.30
GeoB 13728-2	295	*Lophelia pertusa*	364	13.194	0.512176 ±0.000015	-9.02 ±0.30
GeoB 13728-2	295	*Lophelia pertusa*	364	13.194	0.512171 ±0.000015	-9.10 ±0.30
GeoB 13730-1	427	*Lophelia pertusa*	338	13.291	0.512185 ±0.000015	-8.83 ±0.30
GeoB 13737-1#1	Surface	*Lophelia pertusa*	299	13.452	0.512174 ±0.000015	-9.06 ±0.30

Table 2

Core	Depth in core (cm)	^{14}C-age (years)	±1σ (years)	Median probability age (ka BP)
SU92-33	0	2770	70	2437
SU92-33	64	7870	90	8280
SU92-33	70	8670	80	9528
SU92-33	74	9510	100	10295
SU92-33	84	9610	90	10389
SU92-33	90	10180	100	11192
SU92-33	120	11710	110	13172

Table 3

Depth in core (cm)	Age (ka BP)	$\delta^{13}C$ *C. pachyderma* (‰ VPDB)	$\delta^{18}O$ *C. pachyderma* (‰ VPDB)	$\delta^{13}C$ *G. bulloides* (‰ VPDB)	$\delta^{18}O$ *G. bulloides* (‰ VPDB)	$^{143}Nd/^{144}Nd$		εNd	
1	2.53	1.08	1.71	-0.6	1.16	0.512195	±0.000015	-8.64	±0.30
10	3.35	1.00	1.67	-0.82	0.90	0.512186	±0.000015	-8.82	±0.30
19.5	4.26	1.06	1.47	-0.55	1.08	0.512191	±0.000015	-8.72	±0.30
29.5	5.18	1.05	1.78	-0.55	1.02	0.512167	±0.000015	-9.19	±0.30
42.5	6.36	0.90	1.81	-0.91	0.84	0.512179	±0.000015	-8.95	±0.30
52.5	7.28	0.97	1.55	-0.80	0.80	0.512194	±0.000015	-8.66	±0.30
61.5	8.10	0.67	1.58	-0.95	1.01	0.512197	±0.000015	-8.61	±0.30
67.5	9.11	1.13	1.65	-1.07	0.80	0.512169	±0.000015	-9.15	±0.30
72.5	10.10	0.78	2.65	-1.27	0.91	0.512184	±0.000015	-8.86	±0.30
77.5	10.33	0.85	2.75	-1.10	0.83	-	-	-	-
81.5	10.37	0.96	2.41	-1.21	0.96	0.512158	±0.000015	-9.36	±0.30
87.5	10.92	0.70	2.71	-0.11	1.43	0.512184	±0.000015	-8.85	±0.30
92.5	11.39	0.77	3.15	-1.00	0.89	0.512151	±0.000015	-9.50	±0.30
95.5	11.59	0.90	2.69	-1.14	1.21	0.512178	±0.000015	-8.98	±0.30
100.5	11.92	0.67	2.78	-0.44	2.11	0.512171	±0.000015	-9.11	±0.30
110.5	12.58	0.96	2.78	-0.86	2.29	0.512189	±0.000015	-8.76	±0.30
115.5	12.91	0.71	2.96	-0.54	2.01	0.512180	±0.000015	-8.94	±0.30
119.5	13.17	0.96	3.09	-	-	0.512161	±0.000015	-9.31	±0.30
129.5	13.83	0.81	2.99	-	-	0.512156	±0.000015	-9.41	±0.30
135.5	14.23	1.05	3.25	-1.16	1.98	0.512167	±0.000015	-9.19	±0.30
135.5	14.23	-	-	-0.94	2.29	-	-	-	-
139.5	14.49	-	-	-0.96	2.51	0.512170	±0.000015	-9.12	±0.30
159.5	15.88	0.91	3.45	-0.81	2.45	0.512153	±0.000015	-9.47	±0.30
169.5	16.54	1.39	4.09	-0.76	3.47	-	-	-	-
179.5	17.20	1.53	4.30	-0.98	3.45	0.512170	±0.000015	-9.12	±0.30
190	17.86	1.46	4.24	-1.10	3.70	0.512168	±0.000015	-9.16	±0.30
198	18.39	1.65	4.39	-1.24	3.24	0.512153	±0.000015	-9.46	±0.30
206	18.78	1.53	4.28	-0.90	3.53	-	-	-	-

Table 4